iScience

CellPress
OPEN ACCESS

Article

Male-specific behavioral and transcriptomic changes in aging *C. elegans* neurons

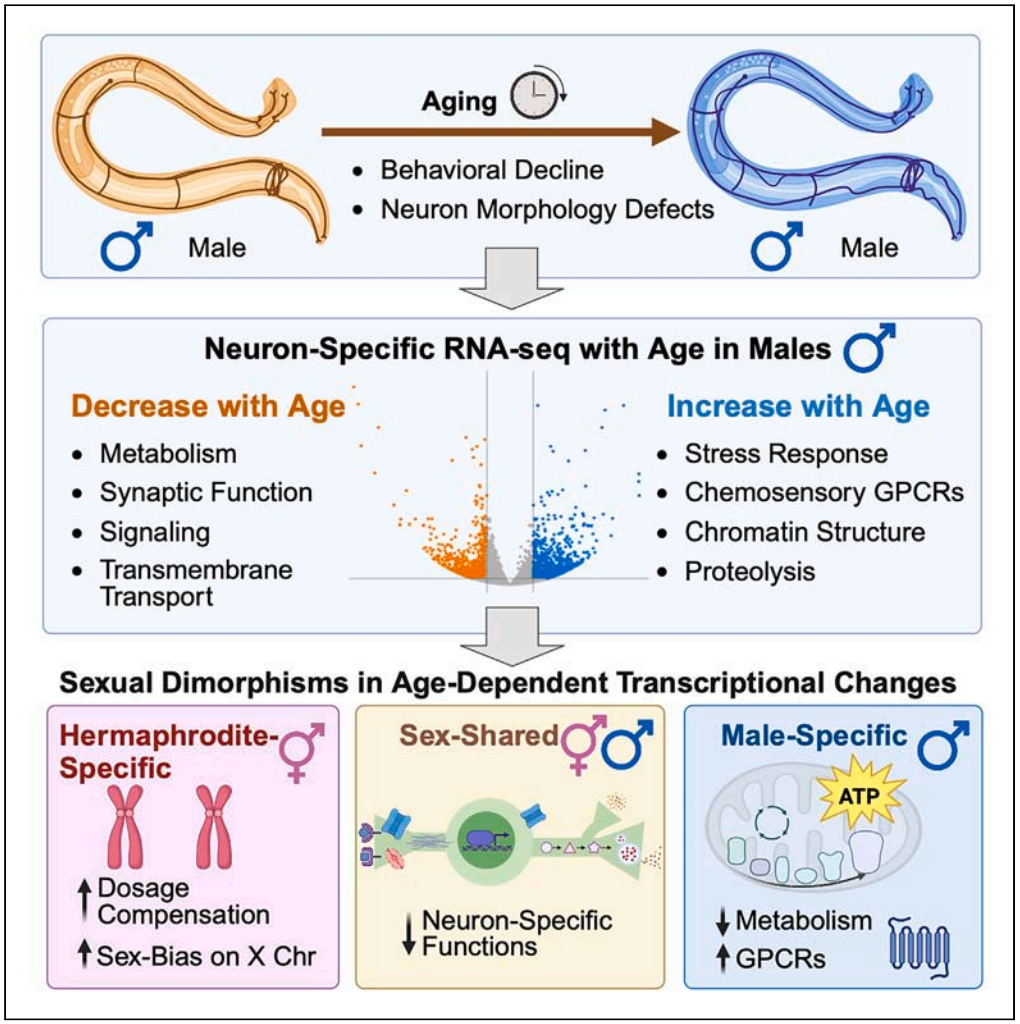

Yifei Weng, Coleen T. Murphy

ctmurphy@princeton.edu

Highlights

Male worms undergo cognitive decline and neuron morphology defects with age

Male neuron RNA-seq uncovers sexual dimorphism in transcriptomic changes with age

X chromosome genes have a greater hermaphrodite bias with age

hrg-7, whose expression declines with age, is required for male sensory behaviors

Weng & Murphy, iScience *27*, 109910
June 21, 2024
https://doi.org/10.1016/j.isci.2024.109910

iScience

CellPress
OPEN ACCESS

Article

Male-specific behavioral and transcriptomic changes in aging *C. elegans* neurons

Yifei Weng[1,2] and Coleen T. Murphy[1,2,3,*]

SUMMARY

Aging is a complex biological process with sexually dimorphic aspects. Although cognitive aging of *Caenorhabditis elegans* hermaphrodites has been studied, less is known about cognitive decline in males. We found that cognitive aging has both sex-shared and sex-dimorphic characteristics, and we identified neuron-specific age-associated sex-differential targets. In addition to sex-shared neuronal aging genes, males differentially downregulate mitochondrial metabolic genes and upregulate GPCR genes with age, while the X chromosome exhibits increased gene expression in hermaphrodites and altered dosage compensation complex expression with age, indicating possible X chromosome dysregulation that contributes to sexual dimorphism in cognitive aging. Finally, the sex-differentially expressed gene *hrg-7*, an aspartic-type endopeptidase, regulates male cognitive aging but does not affect hermaphrodites' behaviors. These results suggest that males and hermaphrodites exhibit different age-related neuronal changes. This study will strengthen our understanding of sex-specific vulnerability and resilience and identify pathways to target with treatments that could benefit both sexes.

INTRODUCTION

Cognitive decline with age is a growing health issue as human life expectancy continues to increase.[1] Sexual dimorphism contributes to the heterogeneity of this process. In humans, women generally outlive men,[2] and various biological markers of aging demonstrate sex differences[3] and are regulated both by sex chromosomes and sex hormones.[4,5] Furthermore, men and women differ in their vulnerabilities in cognitive decline, suggesting biological sex may contribute to the heterogeneous nature of aging. The nervous system is an important target of aging, not only affecting lifespan but also affecting the quality of life, and brain aging also exhibits sex-specific features. Women exhibit slower biological brain aging,[6,7] less structural damage,[8] and decreased cognitive ability decline.[9,10] In addition, men and women show different frailty toward neurodegenerative diseases.[11] However, a comprehensive molecular characterization is required to compare the neuronal aging trajectory between sexes.

Caenorhabditis elegans lives for 2-3 weeks, and displays many quantifiable aging phenotypes during this time.[12–16] *C. elegans* populations are primarily hermaphroditic, but about one in 500 *C elegans* is a male under unstressed conditions.[17] Both sexes have invariant, stereotyped nervous systems that have been fully mapped.[18] The two sexes have 294 common neurons, 8 hermaphrodite-specific neurons, and 91 male-specific neurons. Even the common neurons display sexual dimorphisms at molecular and circuit levels.[19] Males and hermaphrodites elicit various behavioral differences, including pheromone preference [20,21], food searching,[22,23] and complex cue decision-making and learning.[24,25] However, how these male-specific behaviors change with age is less well studied; previous neuronal aging studies have focused primarily on hermaphrodites.[26,27] Male mating ability declines early in adulthood due to increased muscle excitability,[28] but how male cognitive functions change with age is less well understood. While whole-animal transcriptomic studies of the male have been done,[29–31] less is known about male neuronal transcriptome changes with age.

In this study, we characterized male neuronal aging phenotypes. We found that male *C. elegans* can carry out positive Pavlovian olfactory learning and memory, and this ability declines with age. Similarly, sex-specific pheromone chemotaxis behavior, which is stronger in males than in females,[20] also declines with age, as does sensory neuron morphology. To determine how gene expression changes may contribute to these age-related changes, we performed neuron-specific RNA-sequencing of Day 2 and Day 8 adult males. We found that metabolic and GPCR expression changes with age in males more than in similarly aged hermaphrodites. We also found that epigenetic regulators are upregulated specifically in the aged hermaphrodite X chromosome. Lastly, we identified a gene that declines with age specifically in males, the aspartic protease *hrg-7*, and found that this gene is required for male cognitive functions. Our work suggests that transcriptomic changes in neurons with age contribute to the behavioral and morphological declines exhibited in aging males.

[1]Department of Molecular Biology, Princeton University, Princeton, NJ 08544, USA
[2]LSI Genomics, Princeton University, Princeton, NJ 08544, USA
[3]Lead contact
*Correspondence: ctmurphy@princeton.edu
https://doi.org/10.1016/j.isci.2024.109910

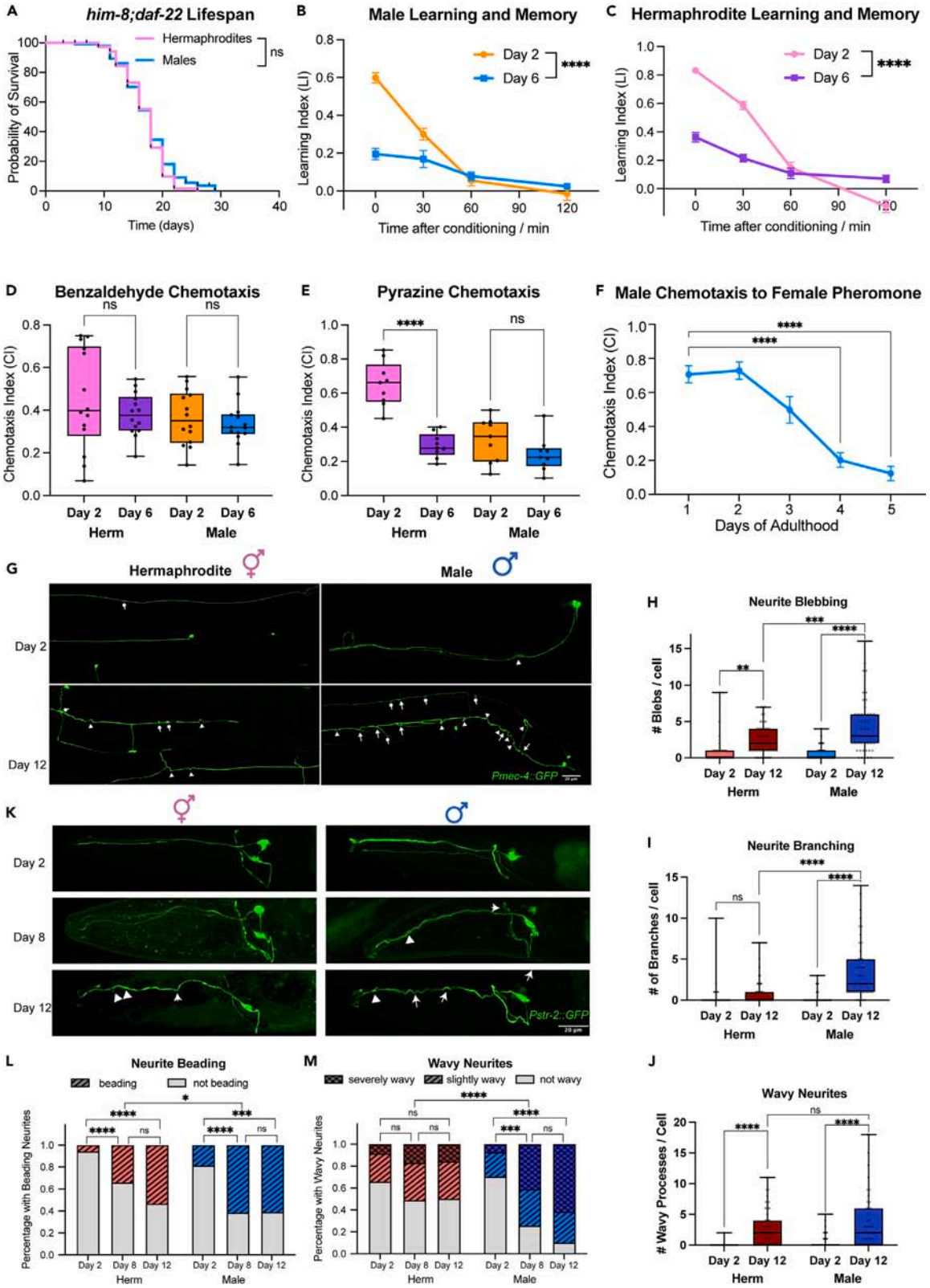
A
him-8;daf-22 Lifespan
Hermaphrodites
Males
ns
Probability of Survival
Time (days)
B
Male Learning and Memory
Day 2
Day 6
****
Learning Index (LI)
Time after conditioning / min
C
Hermaphrodite Learning and Memory
Day 2
Day 6
****
Learning Index (LI)
Time after conditioning / min
D
Benzaldehyde Chemotaxis
ns
ns
Chemotaxis Index (CI)
Day 2
Day 6
Day 2
Day 6
Herm
Male
E
Pyrazine Chemotaxis
****
ns
Chemotaxis Index (CI)
Day 2
Day 6
Day 2
Day 6
Herm
Male
F
Male Chemotaxis to Female Pheromone
****
****
Chemotaxis Index (CI)
Days of Adulthood
G
Hermaphrodite
Male
Day 2
Day 12
Pmec-4::GFP
H
Neurite Blebbing
**
***
****
Blebs / cell
Day 2
Day 12
Day 2
Day 12
Herm
Male
K
Day 2
Day 8
Day 12
Pstr-2::GFP
I
Neurite Branching
ns
****
****
# of Branches / cell
Day 2
Day 12
Day 2
Day 12
Herm
Male
L
Neurite Beading
beading
not beading
*
****
****
***
****
ns
****
ns
Percentage with Beading Neurites
Day 2
Day 8
Day 12
Day 2
Day 8
Day 12
Herm
Male
M
Wavy Neurites
severely wavy
slightly wavy
not wavy
****
ns
ns
ns
***
****
ns
Percentage with Wavy Neurites
Day 2
Day 8
Day 12
Day 2
Day 8
Day 12
Herm
Male
J
Wavy Neurites
ns
****
****
Wavy Processes / Cell
Day 2
Day 12
Day 2
Day 12
Herm
Male

Figure 1. Male neuronal aging can be characterized through aging phenotypes

(A) Lifespan of *him-8;daf-22* males and hermaphrodites. ns: $p > 0.05$, Gehan-Breslow-Wilcoxon test.

(B) Male learning and short-term associative memory (STAM) ability are high in young worms and decrease in aged worms.

(C) Hermaphrodite learning and STAM ability are high in young worms and decrease in aged worms. (B and C) Chemotaxis index at 0 min after conditioning measures learning, and 30 min, 60 min, and 120 min measures short-term memory trajectory. $N = 4$ biological replicates, 5 chemotaxis plates per biological replicate. Error bar denotes ± SEM. ****: $p < 0.0001$, two-way ANOVA with Tukey post-hoc analysis.

(D) Benzaldehyde chemotaxis ability in young and aged animals in both sexes.

(E) Pyrazine chemotaxis ability in young and aged animals in both sexes. (D-E) Each dot represents a chemotaxis plate. $N = 3$ biological replicates. Ns: $p > 0.05$, two-way ANOVA with Tukey post-hoc analysis. Box plots: center line, median; box range, 25-75th percentiles; whiskers denote minimum-maximum values.

(F) Male chemotaxis toward pheromone decreases with age. Chemotaxis index at different ages measures male preference for female pheromones. $N = 3$ biological replicates, 5 chemotaxis plates per biological replicate. ****: $p < 0.0001$, two-way ANOVA with Tukey post-hoc test. (B,C,F) Error bars denote ±SEM.

(G) Representative images of mechanosensory neuron morphology with age. Sex and age of the animal labeled in the image. Arrow: spontaneous branching of the neurite. Arrowhead: wavy processes of the neurite. Round arrow: blebbing of the neurite. Herm: hermaphrodites. Scale bar: 20 μm.

(H-J) Quantification of average blebbing (H) , branching (I), and wavy (J) events per neuronal cell. $N = 23, 26, 39, 32$ animals respectively. ****: $p < 0.0001$, ***: $p < 0.001$, **: $p < 0.01$, ns: $p > 0.05$, One-way ANOVA with Tukey's post-hoc analysis. Boxplots: center line, median; box range, 25-75th percentiles; whiskers denote minimum-maximum values.

(K) Representative images of AWC neuron morphology on Day 2, Day 8, and Day 12. Arrow: wavy neurites. Arrowhead: Beading and branching. Scale bar: 20 μm. See also Figure S1.

(L and M) Quantification of neurite beading and wavy neurite phenotypes in both sexes. $N = 35,41,45,27,39,41$ respectively. ****: $p < 0.0001$, **: $p < 0.01$, *: $p < 0.05$, ns: $p > 0.05$. Chi-square test.

RESULTS

Male neuronal aging in behavior and neuron morphology

Since wild-type males raised together exhibit shortened lifespans due to male pheromone,[32] we used a pheromone-production defective mutant, daf-22, to measure normal aging in males, in a background that produces high incidence of males (*him-8*). We find that him-8; daf-22 males have a lifespan similar to hermaphrodites from the same strain, which indicates the strain is appropriate for aging experiments (Figure 1A).

Next, we assessed male learning and memory using an assay of Pavlovian association between food and butanone.[26,33] On Day 2 of adulthood, males demonstrated intact appetitive learning and memory functions that lasted for about 60 min (Figure 1B); however, there was a significant decline in these abilities by Day 6 (Figure 1B), which is comparable to that observed in hermaphrodites (Figure 1C). This suggests that young males have cognitive functions that are similar to those of hermaphrodites, and that male neuronal aging takes place on a similar trajectory.

To assess whether this behavioral decline was due to chemosensory ability decline, motility decline, or learning and memory ability decline, we tested male and hermaphrodites' chemotaxis to benzaldehyde and pyrazine. We found that aged worms are still able to chemotax toward strong attractants such as benzaldehyde (Figure 1D) and pyrazine (Figure 1E), indicating that their chemosensory and motor abilities are intact. Thus, the learning and memory decline that we see at Day 6 are not due to declines in chemosensory or motility abilities.

C. elegans males display a preference for both hermaphrodite and female ascaroside pheromones,[20,34] but whether this ability declines with age had not been characterized. Using *Caenorhabditis remanei* (true female) pheromones, we investigated males' ability to chemotaxis toward these pheromones as they age. Day 1 males have a strong preference toward female pheromone. However, this attraction declines with age. By Day 4, males lose their ability to chemotaxis toward female pheromone, coinciding with the time frame of their reduced mating capability[22,35] (Figure 1F).

Next, we characterized morphological changes that accompany the observed behavioral decline with age. Mechanosensory neurons have been previously analyzed for morphological changes with age,[13,36–38] but only hermaphrodite neurons were characterized. Here we imaged male mechanosensory neurons with age and compared them to hermaphrodites. Similar to previous findings in hermaphrodites,[36–38] we found that mechanosensory neurons in males also exhibit morphology decline with age (Figure 1G). We found that aged neurons exhibit more neurite blebbing, branching and wavy neurites (Figures 1H–1J). Moreover, hermaphrodites have a less severe phenotype than males in neurite blebbing and branching, which correlate with the more benign changes in hermaphrodite AWC chemosensory neurons.

In addition to mechanosensory neurons, we are interested in examining morphological changes that may accompany the loss of learning and behavior, which are mediated by chemosensory neurons.[26,27,39] AWC neurons are chemosensory neurons responsible for butanone sensation, and these neurons are required for short-term associative memory.[27,40] In both hermaphrodites and males, AWC neurons exhibit their characteristic enlarged dendritic terminals (Figure S1). We found that AWC neurons exhibit an increase in neurite beading and wavy neurites as they age (Figure 1K). Notably, the severity of neurite beading and the wavy neurites in aged males was greater than that observed in age-matched hermaphrodites (Figures 1K–1M). These findings suggest that neuronal aging in males presents some unique, sex-specific features when compared to hermaphrodite aging.

The male neuronal aging transcriptome

To understand the molecular mechanisms that may underlie the behavioral changes with age that we observed, we performed neuron-specific sequencing on Day 2 and Day 8 male neurons. Through filtering separation, we were able to separate males and hermaphrodites from a

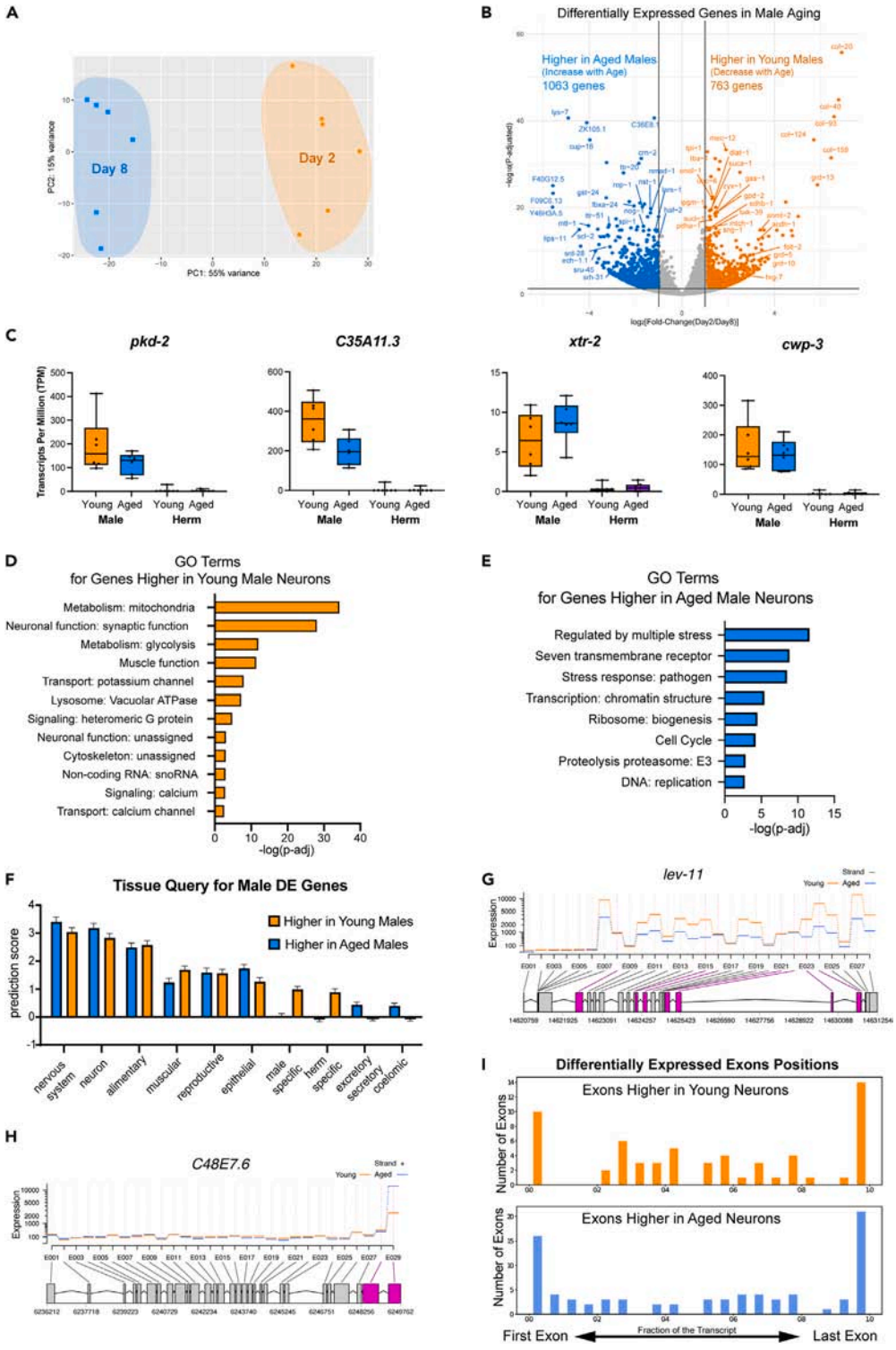

Figure 2. Male neuron sequencing identified gene expression change with age

(A) PCA plot shows age-related separation between young and aged male neuron collections. PCA plot generated using the DESeq2 package.

(B) Volcano plot showing differentially expressed genes in male aging. Log2(fold-change) >1.0 or < -1.0, p-adj <0.05 are considered differentially expressed. Top differentially expressed genes are labeled.

Figure 2. *Continued*

(C) Expression level of representative male-specific genes in males and hermaphrodites. The y axis denotes counted transcripts per million transcripts (TPM) in each sample. Each dot represents one biological replicate in the sequencing. Boxplots: center line, median; box range, 25-75th percentiles; whiskers denote minimum-maximum values.

(D) Gene Ontology (GO) results from genes significantly more highly expressed in young male neurons compared with aged male neurons. Gene ontology generated from Wormcat 2.0 category 2.

(E) GO results from genes significantly more highly expressed in aged male neurons compared with young male neurons. Gene ontology generated from Wormcat 2.0 category 2.

(F) Tissue query for male differentially expressed genes. Top 500 genes more highly expressed in young male neurons or aged male neurons are input for the tissue query. Only prediction scores for major tissues and neuron are shown. Prediction scores and SEM are generated from the tissue query website. Error bars denote ±SEM.

(G and H) Alternative exon usage with age results from DEXSeq algorithm. Each line represents an exon in the gene and the height of the line represents the normalized expression level. The transcript construct is shown below the graph. Exons with alternative change compared to the whole gene is shown in magenta.

(I) Histogram of the positions of the differentially used exons in a gene. The x axis denotes the position of an exon in a gene, where 0 corresponds to the 1st exon, and 1 corresponds to the last exon. The y axis denotes the number of genes differentially used in a certain position in a gene. See also Figure S2.

mixed sample and achieved >95% purity of male worms in our samples, thus making it possible to assess the male neuronal transcriptome using our previously published sorting and sequencing methods.[41–44] PCA of our neuronal RNA-sequencing samples showed a clear separation of the young and aged male neurons (Figure 2A), suggesting that age-related differences were the dominant source of differential gene expression, and the batch effects of the samples are small. Differential expression analysis using DESeq2 identified 763 genes that were more highly expressed in young than aged male neurons and 1,063 genes that were more highly expressed in aged than young male neurons ($\log_2$(fold-change) >1.0 or < −1.0 and p-adj <0.05) (Table S1; Figure 2B).

As a control for our male data, we examined the expression of canonical examples of male-specific genes[29] in both our male and hermaphrodite datasets (Figure 2C). These genes are enriched in and correlate with male neuronal function; for example, PKD-2 is a calcium channel expressed in the CEM neuron and required for male mating,[45] C35A11.3 is enriched in ciliated neurons,[46] XTR-2 is involved in germline sex determination and is predicted to enable transmembrane signaling receptor activity,[47] and CWP-3 is a polycystin-dependent signal transduction protein responsible for sensory functions in the male tail neurons.[48] The fact that we can detect the expression of these genes in male neurons but not in hermaphrodite neurons indicates that our dataset is sensitive enough to detect male-specific transcripts.

Next, we used Gene Ontology (GO) analysis to assess the predicted functions of differentially expressed genes with age. Genes more highly expressed in young male neurons were enriched in GO terms related to mitochondrial metabolism (e.g., *idhg-2, gpd-2, ctc-2*), neuronal synaptic function (e.g., *nlp-20, rab-3, dat-1*), signaling and transport (e.g., *egl-20, twk-30, ccb-2*), and structural and cytoskeletal proteins (e.g., *col-20, col-40, tnt-2*) (Figure 2D). The age-related decline in expression of these genes that are essential to neuronal cell function correlates with the behavioral and morphological declines we noted in aging males.

By contrast, genes higher in aged neurons are enriched in GO terms for stress response (e.g., *mtl-1, cyp-14A5, lys-7*), transmembrane serpentine receptors (e.g., *sru-45, srh-31, srd-28*), and transcription regulation (e.g., *eef-2, his-42, set-32*) (Figure 2E). The increased expression of these genes may suggest transcriptional dysregulation and a response to increased stress in aged neurons. A tissue-specific query showed that these differentially expressed genes had high prediction scores for the nervous system and neurons, validating that our differential expression dataset is neuron-specific (Figure 2F).

We were interested in whether splicing changes with age, so we examined exon and UTR usage changes.[43] We did find examples of exon usage changes with age (Figures 2G and 2H), indicating possible alternative splicing and isoform enrichment in aged neurons, but the direction was not consistent. For example, gene *lev-11* is downregulated with age, not all of its exons are differentially expressed with age (Figure 2G). Another example is gene *C48E7.6*, where most of the exons are not differentially expressed with age, but the last exon increased expression in aged neurons (Figure 2H). In total, we identified 62 exons that are more highly expressed in young neurons, and 82 exons more highly expressed in aged neurons compared to other exons in the gene (Table S2, $\log_2$FC > 1 or < -1, p-adj <0.05). Notably, 34% of the exons higher in young neurons and 45% higher in aged neurons are in the first or the last exon (Figures 2H and 2I), due to changes in the UTR. We identified 188 3′ UTRs and 239 5′ UTRs higher expressed in young neurons, and 317 3′ UTRs and 362 5′ UTRs more highly expressed in aged neurons (Table S2, $\log_2$FC > 1 or < -1, p-adj <0.05). About 20% of the UTRs that are downregulated and 30% of UTRs that are upregulated with age belong to genes that are not differentially expressed with age (Figure S2), indicating that these UTRs harbor different changes than the genes and the open-reading frames. This may indicate alternative regulatory controls of the UTR with age, echoing the Sudmant et al. 2018 finding that 3′ UTRs accumulate in the aged brain due to impaired ribosome recycling[49] and the Chen et al., 2014 finding that senescent cells exhibit global 3′ UTR lengthening.[50]

Comparison with hermaphrodite neuron-specific sequencing reveals sex-specific features

To understand the sex-specific differences between hermaphrodite and male neuronal aging, we compared young and aged hermaphrodite neurons[44] to our newly generated young and aged male neuronal transcriptomes. Samples from males and hermaphrodites distinctly separate along PC1, while PC2 captures age-induced variations (Figure 3A); biological replicates clustered together, indicating the differences we see in expression were not due to sample collection artifacts. We note that the hermaphrodite young and aged samples showed a greater separation than the male samples. This difference may be due to the difference in collection age for the neurons: while hermaphrodite young

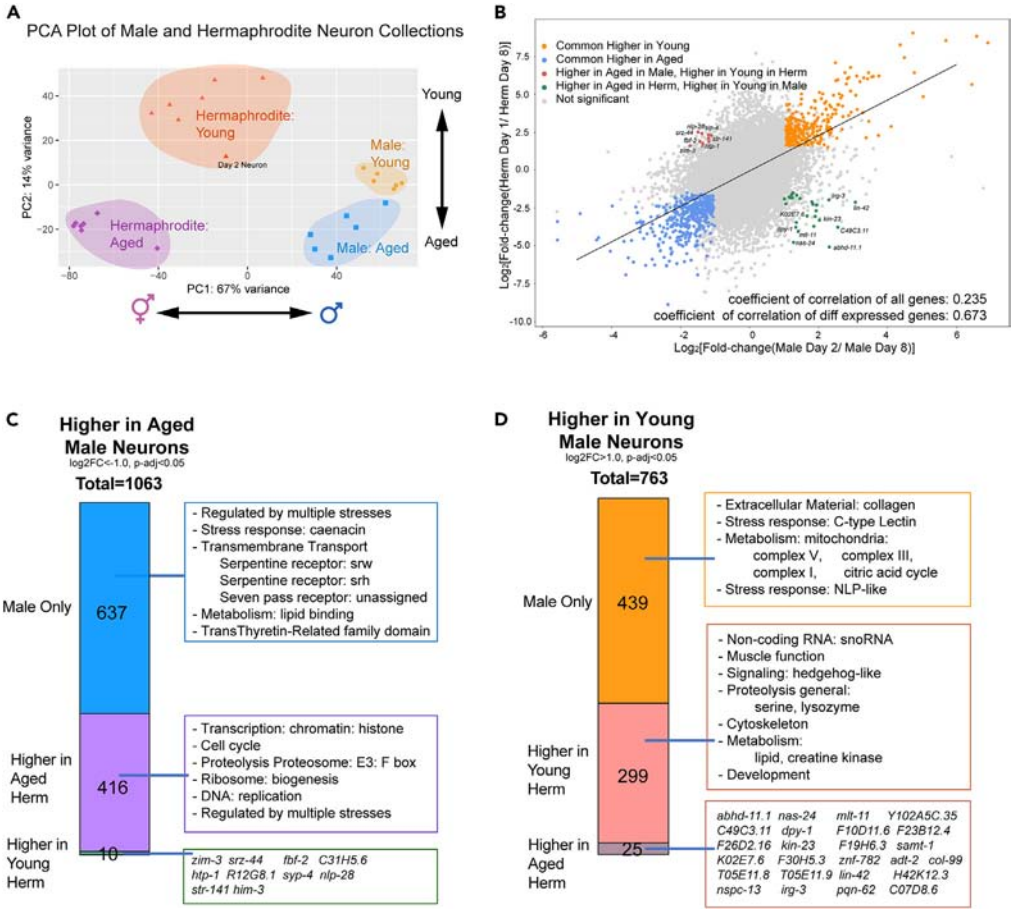

Figure 3. Sex-specific dimorphism in the neuronal aging transcriptome

(A) PCA plot of hermaphrodite and male neuron collection samples. 6 replicates of wild-type hermaphrodites and 1 replicate of *him-8;daf-22* hermaphrodite (Labeled as Day 2 neuron) is shown. The plot is generated from the DESeq2 package.

(B) Correlation of $\log_2$[fold-change(young/aged)] in hermaphrodites (y axis) and males (x axis). Differentially expressed gene cutoff is $\log_2$[fold-change(young/aged)] > 0.5 or < −0.5, p-adj <0.05. Genes differentially expressed are color-labeled as shown.

(C and D) Fraction of male genes more highly expressed in young neurons (C) and aged neurons (D) that are either only differentially expressed in males, or also higher expressed in young neurons in hermaphrodites, or also higher expressed in aged neurons in hermaphrodites. Herm: hermaphrodites. Gene ontology results from WormCat 2.0 category 2. See also Figure S3.

neurons were sorted on Day 1, male neurons were sorted on Day 2 due to the filtration protocol. To control for the age-related differences, we included a Day 2 hermaphrodite neuron collection, and this sample demonstrated a PC2 value comparable to that of the male Day 2 neuron samples (Figure 3A).

Next, we analyzed the correlation of young vs. aged differential gene expression fold-change in hermaphrodites and males (Table S3; Figure 3B). The correlation between the significantly differentially-expressed genes in hermaphrodites and males was high, while the genes not significantly differentially expressed had a lower correlation. This suggests that hermaphrodites and males share many age-related gene expression changes, forming a conserved aging process across both sexes (Figure 3B, orange and blue). Although highly correlated, there is a small set of genes that are differentially expressed in the opposite direction between hermaphrodites and males (red, green on plot). Some genes show higher expression in young hermaphrodite neurons but are increased in aged male neurons, such as *zim-3, srz-44,* and *fbf-2.* Conversely, *lin-42, irg-3,* and *kin-23* among others exhibit higher expression in young male neurons and aged hermaphrodite neurons (Table S4).

Although some enriched GO terms are shared between aging male and hermaphrodite neurons (including transcription, cell cycle, proteostasis, stress responses, ribosome biogenesis, and DNA replication), there were a few notable differences (Figures 3D, 3E and S3). Genes with a higher expression in young neurons in both sexes are enriched in cytoskeletal organization, proteolysis, and lipid metabolic functions. However, genes that are elevated in young male neurons but not in hermaphrodite neurons are associated with mitochondrial metabolism, including Complex I, III, IV, and citric acid cycle genes (Figure 3C). This suggests a decline in cellular respiratory and energy-generating processes, particularly in male neurons as they age. Conversely, genes that exhibit higher expression with age in both sexes show enrichment in

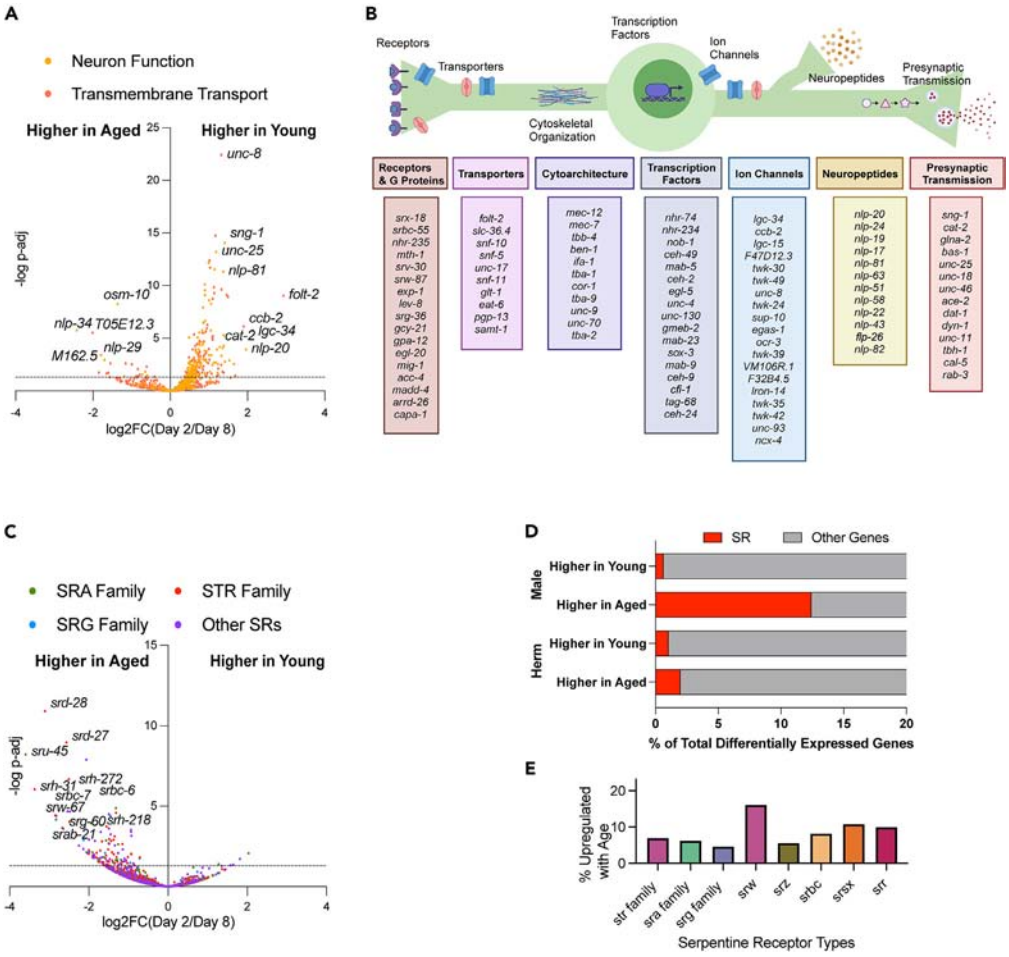

Figure 4. Neuronal genes are differentially expressed with age in males

(A) Volcano plot of neuron functional genes and transmembrane transport genes' expression change with age in males. log_2(Fold-change) and p-adj values from the DESeq2 algorithm.

(B) Neuron function and transmembrane transport genes that downregulate with age in males play various roles in a neuron.

(C) Volcano plot of serpentine receptor (SR) genes' expression change with age in males. log_2(Fold-change) and p-adj values from the DESeq2 algorithm.

(D) Percentage of SRs that are differentially expressed with age in males and hermaphrodites.

(E) Percentage of SRs in each SR family that are upregulated with age in males. See also Figure S4.

proteolysis proteasome and epigenetic modification pathways, but genes that are only upregulated in aged male neurons additionally demonstrate a marked enrichment in seven-transmembrane receptors, most of which are serpentine receptors (Figures 3D, S4C, and S4D).

Neuronal functional genes are higher in young neurons in both sexes

Very few neuronal genes are upregulated with age (Figures 4A and S2A), but among those were genes encoding two neuropeptides (*nlp-34* and *nlp-29*) and OSM-10, which is known to be expressed in sensory neurons in the hermaphrodite.

Perhaps unsurprisingly, we found that neuronal functional genes for the most part decline with age in both hermaphrodite and male neurons (Figures S4A and S4B). These neuronal genes participate in various aspects of neuronal function, including signaling, transport, transcription, and cytoskeletal architecture (Figure 4B). Genes higher expressed in young neurons include postsynaptic receptors and G-protein signaling pathway genes, such as the *srx-18, srbc-55, srv-30, srw-87, srg-36, Methuselah/mth-1,* and *capa-1* GPCRs (although the majority of serpentine receptors are upregulated with age - see below and Figure 4C), nuclear hormone receptor *nhr-235*, neurotransmitter receptors *exp-1, lev-8,* and *acc-4*, receptor tyrosine kinase *egl-20*, WNT receptor *mig-1*, axon guidance receptor *madd-4*, and the heteromeric G proteins *gpa-12, gcy-21*, and *arrd-26*. Transmembrane porters and ion channels are also more highly expressed in young male neurons, including potassium channels *twk-30, twk-49, F47D12.3, twk-24, twk-39, sup-10, VM106R.1, F32B4.5, unc-93, twk-35, twk-42,* and *Iron-14*, calcium channels *ccb-2, ocr-3, ncx-4*, sodium channels *unc-8, egas-1*, ligand-gated channels *lgc-34, lgc-15*, amino acid transporters *slc-36.4, snf-10, glt-1,*

GABA transporter *snf-5, snf-11*, ATPase-coupled transporter *pgp-13*, molybdate ion transporter *samt-1*, and sodium:potassium–exchanging transporter *eat-6*.

There are also genes that regulate the cytoskeletal architecture that decline with age, including tubulins *mec-12, mec-7, tbb-4, ben-1, tba-1, tba-9*, and *tba-2*, intermediate filament *ifa-1*, and actin filament binding proteins *cor-1, unc-9*, and *unc-70*. Neuronal transcription factors *ceh-2, egl-5, unc-4, unc-130*, and *ceh-4*, and neuropeptides, including *nlp-20, nlp-24, nlp-19*, and *nlp-17* also decline with age.

Synaptic proteins, including synaptic vesicle formation and release proteins *sng-1, unc-18, unc-46, dyn-1, unc-11, cal-5, rab-3*, and neurotransmitter synthesis and uptake enzymes *cat-2, glna-2, bas-1, unc-25, ace-2, dat-1*, and *tbh-1* also decline with age. Overall, this wide range of neuronal genes being downregulated with age may predispose the neurons to be unable to fulfill various cellular processes such as gene regulation, structural integrity, signal propagation, and synaptic transmission, thus leading to the behavioral and morphological changes we see in aged animals.

Chemosensory GPCRs are upregulated in aged neurons in males

We also found that chemosensory GPCRs, especially serpentine receptors, were upregulated with age in male neurons (Figure 4C). In fact, about 10% of all genes that were upregulated with age were serpentine receptors (Figure 4D). This is a phenomenon specific to males: serpentine receptors are not similarly enriched in genes that upregulate in aged hermaphrodite neurons (Figures S4C and S4D). The serpentine receptors that are upregulated with age include all major serpentine receptor classes, including *str*, *sra*, and *srg* superfamily genes, *srw, srz, srbc, srsx*, and *srr* families (Figure 4E). The differential expression of these serpentine receptors, which plays a crucial role as chemosensory GPCRs, may underlie the behavioral differences of odorant sensation and chemotaxis in males and hermaphrodites.[51,52]

Canonical metabolic genes are downregulated with age in male neurons

One category of genes that decline specifically in aging male neurons but not in aging hermaphrodite neurons are those involved in canonical energy-generating respiratory metabolic pathways (Figures 5A, S4E, and S4F). Mitochondrial-related genes are more highly expressed in young male neurons (Figures 2C and 5A): glycolytic and mitochondrial metabolic genes are enriched in GO categories for genes more highly expressed in young male neurons. We found that several enzymes of that mediate glycolysis are downregulated with age at least 2-fold (labeled in red) (Figure 5B), including 6-PhosphoFructoKinase *pfk-1.1*, 6-PhosphoFructoKinase *aldo-1*, glyceraldehyde-3-phosphate dehydrogenase *gpd-2*, phosphoglycerate mutase *ipgm-1*, phosphoglycerate mutase *enol-1*, and pyruvate dehydrogenases *pdha-1, pdhb-1, dlat-1, dlat-2*, and *dld-1*. Mitochondrial metabolic genes are also significantly downregulated, including TCA cycle enzymes *idhg-2, dlst-1, dld-1, sucl-1, suca-1, sdha-1, sdhb-1, sdhd-1*, and *mdh-1*, and electron transport chain complex subunits for each complex. This includes Complex 1 (ubiquinone) genes *gas-1, nduo-3, Y54F10a.m.5, Y63D3A.7, F31D4.9, lpd-5, nduo-6, C33A12.1, Y71H2a.m.4, C18E9.4*, and *nduo-4*; Complex II (succinate dehydrogenase) genes *sdha-1, sdhb-1*, and *sdhd-1*; Complex III (Coenzyme Q – cytochrome c) and cytochrome *c* genes *F45H10.2, cyc-1, ucr-11, ctb-1, ucr-2.2,T02H6.11*, and *C14B9.10;* Complex IV genes, *ctc-2, cox-6c, cox-4*, and *cox-6b*; and ATP synthase subunits *asb-2, R04F11.2, asg-2, Y82E9BR.3, Y69A2AR.18, atp-2, atp-1*, and *R53.4* (Figures 5B and 5C). The downregulation with age of these fundamental carbohydrate metabolic genes may impose a sex-unique challenge to male neuronal metabolism in aged animals.

To understand whether this sex-specific downregulation of metabolic genes is due to young males having higher expression of metabolic genes than hermaphrodites, or due to aged males expressing lower levels of metabolic genes, we compared the correlation of transcript number per million transcripts (TPM) of metabolic genes between hermaphrodites and males (Figure 5D). We found that in young animals, males and hermaphrodites have a good correlation of mitochondrial-related gene expression (although hermaphrodites have slightly higher expression), but hermaphrodites have even higher metabolic gene expression than males in aged animals. Thus, the decline of metabolic genes in aged animals is not due to a high expression of metabolic genes in young animals, but a decline in expression of metabolic genes in aged animals, thus very likely compromising their energy production and cellular activity maintenance.

X chromosomal genes exhibit changes with age

The sex chromosome (X) contributes genetically to sex differences; thus, we focused on the X chromosomal changes during neuronal aging of hermaphrodites and males. In C. elegans, hermaphrodites possess two X chromosomes (XX), whereas males have just one (XO).[53] To counteract this imbalanced chromosome number, worms carry out dosage compensation mechanisms to ensure a balanced expression of X chromosomal genes across both sexes.[54] Dosage compensation should be maintained throughout life to achieve normal gene expression levels. Therefore, we analyzed the expression of all of the chromosomes with age, and further, expression of X chromosome genes in both males and hermaphrodites. We found that in all autosomes, there is male-biased gene expression in young neurons, meaning genes on that chromosome are more likely to be higher expressed in males than hermaphrodites, and this male bias declines in aged neurons (Figures 6A and S3A). However, in the X chromosome, there is not a significant sex bias in young neurons, and there is a hermaphrodite bias in the aged neurons (Figure 6A).

Among all the chromosomes, the X chromosome has the highest enrichment of neuron function genes, indicating it as a potentially vital regulator in cognitive aging, regardless of sex (Figures 6B and S3B). However, we observed an age-related upregulation of dosage compensation complex genes only in hermaphrodite neurons (Figures 6C and S3C). This suggests a potential dysregulation of the dosage compensation/X inactivation process in aged hermaphrodites, which may contribute to sex-specific changes with age in X chromosomal genes only in hermaphrodites.

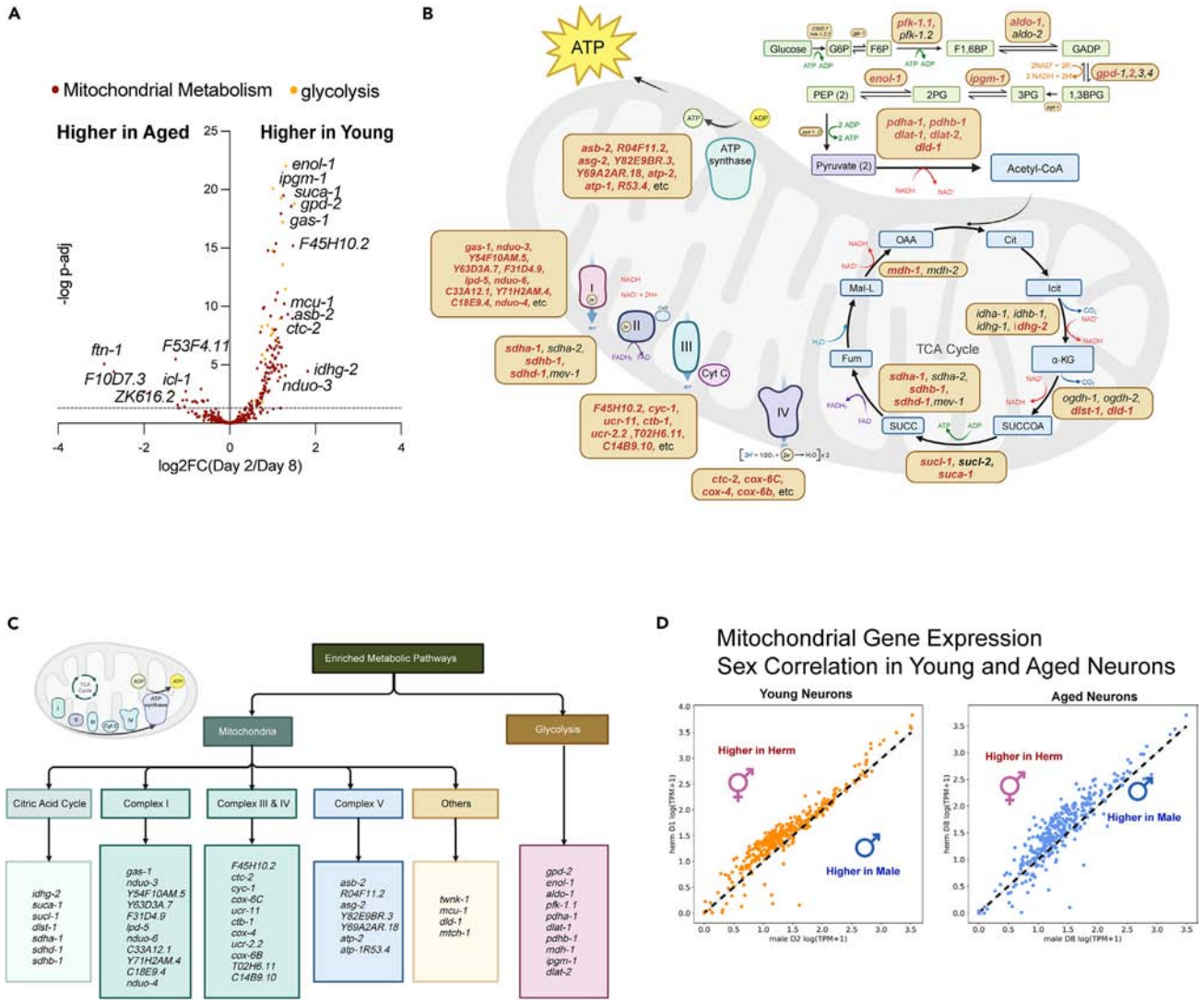

Figure 5. Mitochondrial genes are differentially expressed with age in males

(A) Volcano plot of mitochondrial metabolic and glycolysis genes' expression change with age in males. log_2(Fold-change) and p-adj values from the DESeq2 algorithm.

(B) Metabolic flux of glycolysis, TCA cycle and electron transport chain. Metabolic enzymes whose gene expression is downregulated with age in male neurons are labeled in red.

(C) Metabolic genes that are more highly expressed in young neurons participate in different metabolic categories.

(D) Correlation of transcript per million (TPM) number mitochondrial metabolic genes in hermaphrodite neuron and male neuron in young and aged animals. Dots above the dashed line indicates expression level is higher in hermaphrodite neurons than male neurons. See also Figure S4.

To test that hypothesis, we plotted the correlation of X chromosomal gene expression in both young and aged neurons. Previously, Albritton et al. found that genes on the X chromosome are more likely to be hermaphrodite-biased in their expression, although in general sex-biased genes are more likely male-biased.[55] In our study, we found that in young neurons, the gene expression levels between hermaphrodite and male neurons correlate well (r^2 = 0.85), suggesting a stable gene expression with minimal sex-specific variances (Figure 6D; Table S5). However, in aged neurons, this correlation decreased greatly (r^2 = 0.63), indicating a sex-specific age-dependent differential regulation of X chromosome genes. Notably, the expression distribution is slightly skewed (skewness = +0.38), with more genes having higher expression in aged hermaphrodites than aged males (Figures 6D and S5A).

We next quantified the number of X chromosome genes that are slightly (2-fold difference), strongly (8-fold difference) or completely sex-specific (expressed only in one sex). We found that on the X chromosome, there are more sex-biased genes expressed in aged neurons than in young neurons, and aged hermaphrodites more strongly express neuronal X chromosome sex-biased and sex-specific genes than do males (Figure 6E).

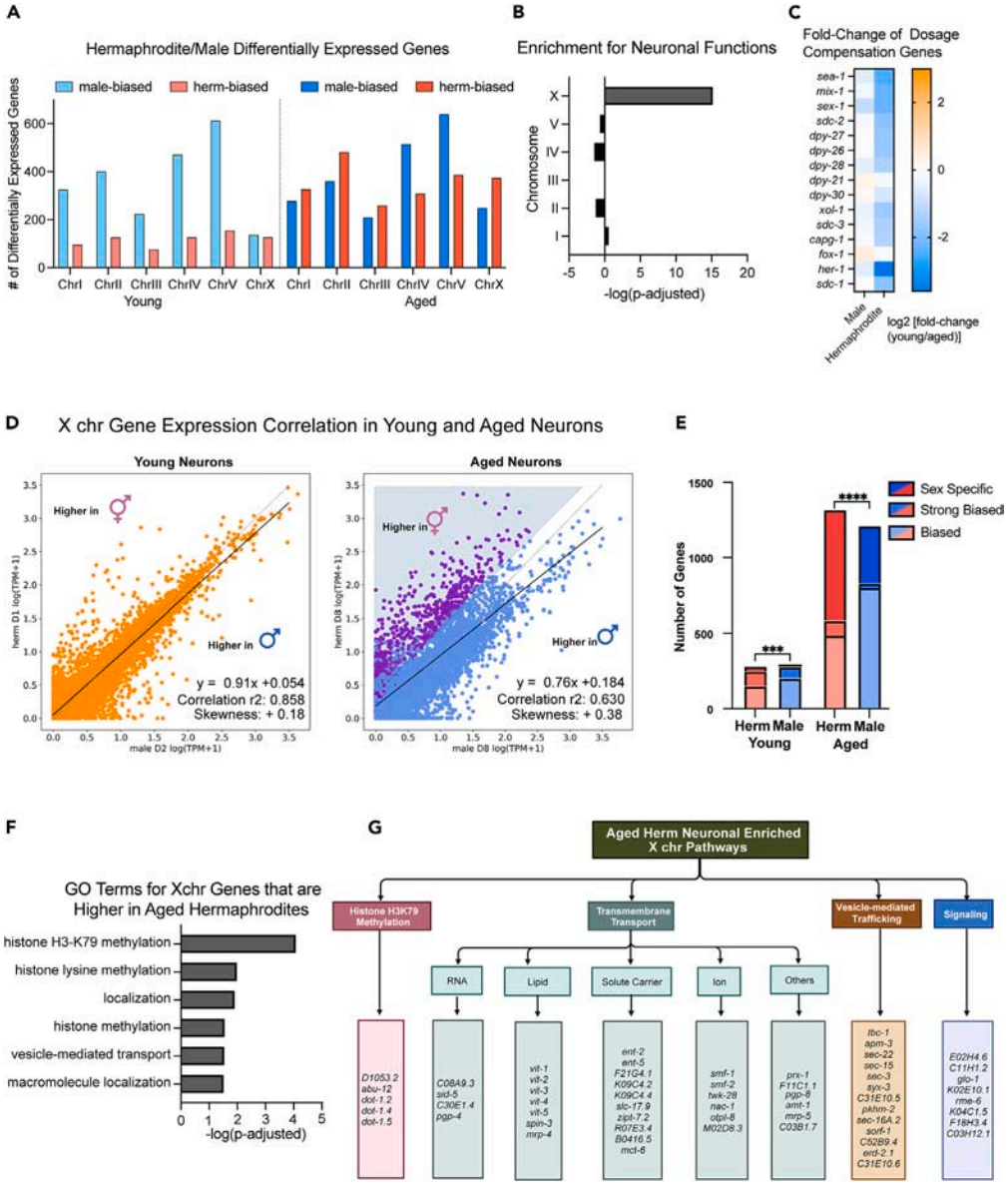

Figure 6. X chromosomal gene regulation exhibits sex-specific dimorphisms

(A) The number of genes significantly expressed between sexes on each chromosome. Male-biased genes are significantly more highly expressed in male neurons compared with aged-controlled hermaphrodites, and hermaphrodite-biased genes vice versa. Genes significantly biased have a log2[fold-change(herm/male)] > 2 or < −2, p-adj <0.05 from the DESeq2 algorithm.

(B) Genes from the X chromosome are enriched in neuronal functions. Gene ontology of all protein-coding genes in a chromosome is used as input for WormCat gene ontology analysis.

(C) log2[fold-change(young/aged)] of dosage compensation complex genes from the DESeq2 algorithm.

(D) Male-hermaphrodite correlation of gene expression on the X chromosome. In young neurons, gene expression correlation between 2 sexes is higher than in aged neurons. Linear regression fitted curve, Pearson's correlation r2, and distribution skewness are calculated using Python. Genes significantly higher expressed in aged hermaphrodites compared with aged males are labeled in purple.

(E) Number of genes that are sex-specific (TPM >1 in one sex, and TPM <0.01 in the other sex), sex-biased (TPM >0.01 in both sexes, and TPM ratio >2, and p-adj <0.05) and strongly sex-biased (TPM >0.01 in both sexes, and TPM ratio >8, and p-adj <0.05). ***: $p < 0.001$, ****: $p < 0.0001$, chi-square tests.

(F) Gene ontology terms for X chromosomal genes that are higher expressed in aged hermaphrodites. GO Terms measured using gProfiler.

(G) Genes belonging to the enriched GO terms from (F). See also Figure S5.

GO term analysis of the X chromosome genes that are significantly more highly expressed in aged hermaphrodites revealed an enrichment in pathways like histone H3K79 methylation and localization (Figure 6F). The "localization" gene ontology term included genes that function in (1) transmembrane transport, including mediating the transportation of RNA (e.g., *sid-5* and *pgp-4*), lipid (e.g., *vit-1*, *spin3*, and *mrp-4*), ions (e.g., *smf-1*, *smf-2*, and *twk-28*), and solute carriers (e.g., *ent-2*, *ent-5*, and *slc-17.9*), and others (e.g., *prx-1*, *pgp-8*, and *amt-1*), (2) vesicle-mediated transport, including in exocytosis (e.g., *sec-15*, *sec-3*, and *syx-3*), endocytosis (e.g., *apm-3* and *sorf-1*), and ER/Golgi trafficking (e.g., *sec-22*, *erd-2.1*, *pkhm-2*, and *sec16A.2*) (3) signaling, including receptors (e.g., *E02H4.6* and *C11H1.2*), and G proteins (e.g., *glo-1*, *rme-6*, and *K02E10.1*) (Figure 6G).

The changes in these X chromosomal genes may contribute to the sexual dimorphic phenotypes we see in aged animals. Histone H3K79 methylation genes may contribute to chromatin regulation of enhancer regions and gene expression,[56,57] while neuronal transport and localization genes may contribute to ion transport and vesicular signaling. Therefore, these X chromosomal differentially expressed genes may play roles in the observed sexual dimorphism in aging behaviors and transcriptomes.

The heme responsive Gene *hrg-7* may be required for young male behaviors

We would hypothesize that genes differentially expressed with age may play an important role in cognitive decline. We tested several genes that significantly decline with age in males (Figure 7A). *acdh-1* encodes an acetyl-CoA dehydrogenase whose expression decreasing with age in both males and hermaphrodites, and *nlp-20* encodes a neuropeptide-like signaling protein that also decreases with age in both sexes. hrg-7, which encodes an aspartic-type endopeptidase, is more highly expressed in young male neurons than in aged male neurons (Figure 2B), and its expression declines more significantly with age in males compared to hermaphrodites (Figure 7A). Lastly, LIN-42 is a transcription factor whose homolog in mammals regulates the circadian rhythm; *lin-42's* expression decreases with age in male neurons but increases with age in hermaphrodites.

We used neuron-specific RNAi to knock down these genes in adults using a strain with a *sid-1* mutation expressing a pan-neuronal *sid-1* rescue (TU3595: *sid-1(pk3321) him-5(e1490) V; lin-15B(n744) X; uIs72 [pCFJ90(myo-2p::mCherry) + unc-119p::sid-1 + mec-18p::mec-18::GFP]*). After treating the animals for two days of adulthood, we tested their learning and memory on Day 3. Reduction of these genes did not induce changes in learning and memory ability, except for *acdh-1* reduction, which had a slight effect on 1 h memory in both males and hermaphrodites (Figures 7B and 7C). We next tested whether these genes participate in male-specific behaviors using the pheromone chemotaxis assay. We found that *hrg-7* knockdown significantly reduces males' ability to chemotaxis to female pheromone (Figure 7D). Then we further examined whether *hrg-7* also affects other behavior in a male-specific manner using chemotaxis to pyrazine. We found that *hrg-7* knockdown reduced chemotaxis to pyrazine specifically in males (Figure 7E). These results indicate a role for HRG-7 specifically in regulating male behaviors and suggest that its age-related decline may contribute to the reduced chemotaxis and pheromone sensing behavior we observed in aged males. *hrg-7* was previously found to be expressed in the intestine, and we have recently discovered that *hrg-7* is also expressed at low levels in a broad set of male neurons in addition to the intestine (Murphy Lab, unpublished). HRG-7 is secreted as an inter-organ signaling protein in hermaphrodites, sending signals from the intestine to the neuron; HRG-7 is thought to be crucial for the regulation of heme homeostasis.[58]

This finding further strengthens the connection between sex-specific transcriptomic changes and behavioral decline during aging. Our results indicate that we can use this dataset to identify genes that contribute to sex-specific phenotypes during cognitive aging, and it will offer valuable insights into sex-specific individualized interventions to regulate cognitive decline in both sexes.

DISCUSSION

Here, we characterized behavioral and morphological changes during male cognitive decline, discovering that male learning and memory function, pheromone preference, and male neuronal morphology integrity all decline with age. We then performed neuron-specific sequencing on young and aged male neurons to identify gene expression changes. We found that neuronal and mitochondrial metabolic genes decrease with age, and some GPCRs and stress-response-related genes increase with age. We then performed a comparison with the hermaphrodite neuron transcriptome both at the genome-wide and X chromosomal levels to identify sexual dimorphic gene expression features with age. Through our sequencing and analysis, we discovered genes that regulate behavioral change with age in a sex-specific manner, linking transcriptomic analysis with behavioral outcomes.

We found that some male neuronal aging phenotypes are more severe than is observed in hermaphrodites. While male learning and short-term memory decline are comparable to that of hermaphrodites, the male's ability to chemotaxis to female pheromone declines starting Day 3, before many behavioral deficits with age observed in hermaphrodites. Males also have a more severe wavy neurite phenotype compared with hermaphrodites in aged neurons. Notably, these phenotypic declines coincide with the timescale of male mating ability decline.[35] We hypothesize that the male cognitive decline can be explained in the evolutionary context. By adult Day 3, male mating potency is significantly decreased,[35] and there may be no survival advantage for individuals with improved cognitive ability post-reproduction. By contrast, hermaphrodites' reproductive ability is maintained until Day 8–10[16,59], so there may be an evolutionary benefit to maintaining hermaphrodite-specific and sex-shared behaviors slightly longer with age.

We also identified male-specific transcriptomic changes with age. We found that metabolic genes, such as *acdh-1*, *abhd-11.1*, *idhg-2*, and *dhs-2*, decline with age in male neurons (Figures 2C and 5). Nervous system metabolism is crucial to the execution of its functions. In humans, the brain consumes 20% of the total energy intake despite being only 2% of the total weight,[60] and females have increased mitochondrial activity and consume more oxygen than their male counterparts at the same age.[61] The human female brain also maintains metabolic youth

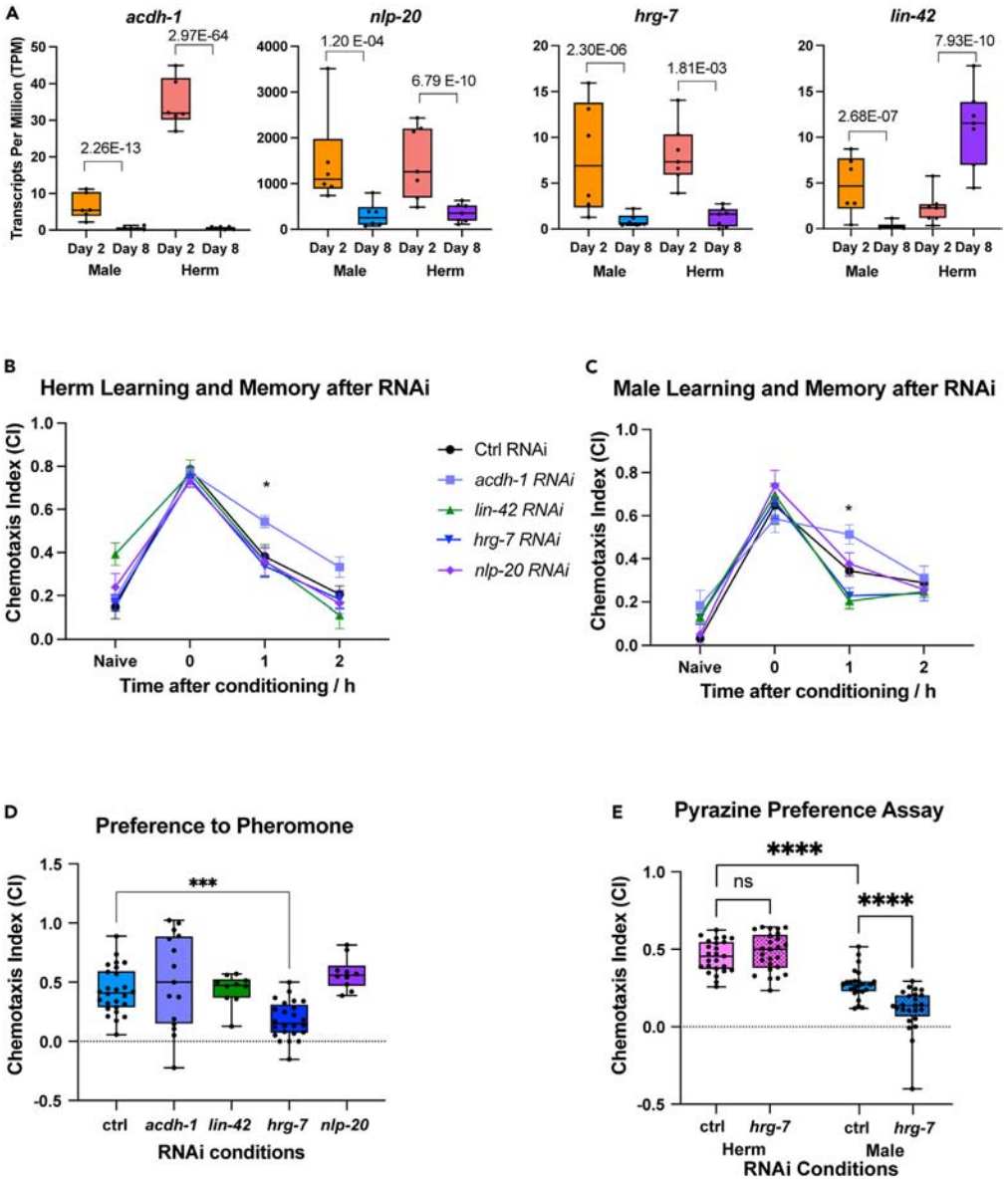

Figure 7. *hrg-7* is required for male-specific chemotaxis functions

(A) *acdh-1, nlp-20, hrg-7 and lin-42* expression level in males and hermaphrodites. The y axis denotes counted transcripts per million transcripts (TPM) in each sample. P-adjusted value from DESeq2. Boxplots: center line, median; box range, 25-75th percentiles; whiskers denote minimum-maximum values.

(B) Hermaphrodite learning and STAM ability under neuron-specific RNAi.

(C) Male learning and short-term associative memory (STAM) ability under neuron-specific RNAi. (B and C) Neuron-specific RNAi was performed using a strain with a *sid-1* mutation and neuronal *sid-1* rescue. The chemotaxis index at 0 min after conditioning measures learning, and 30 min, 60 min, and 120 min measures short-term memory trajectory. $N = 2$ biological replicates, 5 chemotaxis plates per biological replicate. *: $p < 0.05$, two-way ANOVA with Tukey post-hoc analysis. Error bars denote $\pm$SEM.

(D) Male's ability to chemotaxis to female pheromone is compromised in *hrg-7* neuron-specific RNAi knockdowns. RNAi is performed in the TU3595 neuron-specific RNAi strain. $N = 3$ biological replicates, 5 chemotaxis plates per replicate. ***: $p < 0.001$, One-way ANOVA with Tukey's post-hoc test.

(E) Pyrazine chemotaxis is compromised in *hrg-7* neuron-specific RNAi knockdown worms, but only in males. $N = 4$ biological replicates, 25 chemotaxis plates total. ****: $p < 0.0001$, ns: $p > 0.05$. One-way ANOVA with Dunnett post-hoc test. (D and E) Boxplots: center line, median; box range, 25-75th percentiles; whiskers denote minimum-maximum values.

better with age compared with the male brain,[7] which is consistent with our observations here in *C. elegans* neurons. Mitochondrial dysfunction is associated with various neurodegenerative diseases.[62,63] Thus, this decrease in metabolic gene expression may pose a sex-specific threat to aged neurons in males.

In addition to genes with decreased expression with age, we also found that male neurons have increased GPCR expression with age, which is not observed in hermaphrodites. Interestingly, many of these GPCRs are not detected in hermaphrodites (e.g., *sru-45, srh-31, srg-60, srh-272*).[64] The sex dimorphic expression of chemosensory GPCRs is not surprising given the chemosensory behavioral differences observed by us and others (Figures 1 and 6). The upregulation of these GPCRs with age, though, is more interesting. Cognitive aging can also be associated with neuronal hyperactivity[65] and the expression of GPCRs could contribute to cellular excitability. Thus, the upregulation of GPCRs may promote neuronal hyperactivity and promote cognitive aging.

In addition to looking at the transcriptomic changes in general, we also focused on the sex chromosome. Here, we found that the X chromosome is enriched in genes with neuronal functions. These include neurotransmitter release and receptors (e.g., *acr-8, acr-12, dop-1*, and *mgl-1*), signal transduction (e.g., *aex-3, mec-2, odr-10*, and *osm-11*), and neuropeptides (e.g., *flp-2, flp-3, flp-5, nlp-1*, and *nlp-2*). Previously, the X chromosome had been noted to express genes in a sex-biased manner[55]; here we further characterized how the X chromosomal gene expression bias in the nervous system changes with age. We found that in all autosomes, there is male-biased gene expression in young neurons, meaning genes on that chromosome are more likely to be higher expressed in males than hermaphrodites, and this male bias declines in aged neurons (Figure S5). However, the X chromosome is different from the autosomes, with a hermaphrodite-biased gene expression profile, and this bias is greater in aged neurons. We then examined individual genes with a hermaphroditic bias on the X chromosome, and found that the genes more highly expressed in hermaphrodites in aged neurons are enriched in H3K79 histone modification, in addition to neuronal signaling genes. In mammals the H3K79 methyltransferase DOTL1 mediates neurogenesis and neuronal energy metabolism.[66,67] DOT1L in *C. elegans* has been shown to regulate H3K9me2 in enhancer regions and regulate RNAi efficiency through suppression of heterochromatin, thus eliciting a global impact on gene expression.[56,57] Interestingly, in mammals, histone modification enzymes are also among the X chromosomal inactivation (XCI) escapee genes that are found to be expressed from the inactivated X chromosome.[68] The expression of the XCI escapee gene, Kdm6a, in males has beneficial effects on cognitive aging.[69] Thus, X chromosomal hermaphroditic bias in gene expression may be a conserved feature, and these biased genes may act to regulate cognitive health with age in hermaphrodites and females. Together, our analyses uncovered genes and pathways that may affect neuronal aging in a sex-specific manner.

Limitations of the study

Our study characterized the male neuronal aging process using behavior paradigms, morphological assessments, and transcriptomes to identify sex-specific differences during neuronal aging. However, we note that this transcriptomic study is performed using tissue-specific bulk sequencing and thus may lack neuron-type-specific data. Future studies on the male transcriptome on the single-cell level will provide more insights into where these gene expression changes occurred in the nervous system, and further design appropriate experiments to test their function in specific neurons.

STAR★METHODS

Detailed methods are provided in the online version of this paper and include the following:

- KEY RESOURCES TABLE
- RESOURCE AVAILABILITY
  - Lead contact
  - Materials availability
  - Data and code availability
- EXPERIMENTAL MODEL AND STUDY PARTICIPANT DETAILS
  - General worm maintenance
  - C. elegans strains
- METHOD DETAILS
  - Chemotaxis and learning and memory assays
  - Pheromone preference assay
  - Neuron morphology imaging
  - Neuron sorting and RNA extraction
  - RNA sequencing and data analysis
- QUANTIFICATION AND STATISTICAL ANALYSIS

SUPPLEMENTAL INFORMATION

Supplemental information can be found online at https://doi.org/10.1016/j.isci.2024.109910.

ACKNOWLEDGMENTS

We thank the *Caenorhabditis* Genetics Center (CGC) and the Hamza Lab for strains, WormBase (version WS289) for information, Jasmine Ashraf, William Keyes, and Titas Sengupta for help with experiments, members of the Murphy Lab for input on the manuscript, Christina DeCoste, Katherine Rittenbach and the Flow Cytometry Facility for cell sorting assistance, Wei Wang and the Genomics Facility for sequencing

assistance, Lance Parsons for insights on data analysis, and Biorender.com for schematic design. C.T.M. is the Director of the Simons Collaboration on Plasticity in the Aging Brain (SCPAB), which supported the work, and the Glenn Center for Aging Research at Princeton. Y.W. is supported by China Scholarship Council (CSC).

AUTHOR CONTRIBUTIONS

Conceptualization, C.T.M.; Methodology, C.T.M. and Y.W., Investigation, Y.W.; Writing – Original Draft, C.T.M and Y.W.; Writing – Review and Editing, C.T.M and Y.W.; Funding Acquisition, C.T.M.; Supervision, C.T.M.

DECLARATION OF INTERESTS

The authors declare no competing interests.

Received: December 18, 2023
Revised: March 20, 2024
Accepted: May 3, 2024
Published: May 8, 2024

REFERENCES

1. Global Status Report on the Public Health Response to Dementia (2021 (World Health Organization).
2. Thornton, J. (2019). WHO report shows that women outlive men worldwide. BMJ *365*, l1631. https://doi.org/10.1136/bmj.l1631.
3. Hägg, S., and Jylhävä, J. (2021). Sex differences in biological aging with a focus on human studies. Elife *10*, e63425. https://doi.org/10.7554/eLife.63425.
4. Gentilini, D., Castaldi, D., Mari, D., Monti, D., Franceschi, C., Di Blasio, A.M., and Vitale, G. (2012). Age-dependent skewing of X chromosome inactivation appears delayed in centenarians' offspring. Is there a role for allelic imbalance in Healthy Aging and Longevity? Aging Cell *11*, 277–283. https://doi.org/10.1111/j.1474-9726.2012.00790.x.
5. Davis, E.J., Broestl, L., Abdulai-Saiku, S., Worden, K., Bonham, L.W., Miñones-Moyano, E., Moreno, A.J., Wang, D., Miñones-Moyano, E., Williams, G., et al. (2020). A second X chromosome contributes to resilience in a mouse model of Alzheimer's disease. Sci. Transl. Med. *12*, 5677. https://doi.org/10.1126/SCITRANSLMED.AAZ5677.
6. Horvath, S., Gurven, M., Levine, M.E., Trumble, B.C., Kaplan, H., Allayee, H., Ritz, B.R., Chen, B., Lu, A.T., Rickabaugh, T.M., et al. (2016). An epigenetic clock analysis of race/ethnicity, sex, and coronary heart disease. Genome Biol. *17*, 171. https://doi.org/10.1186/s13059-016-1030-0.
7. Goyal, M.S., Blazey, T.M., Su, Y., Couture, L.E., Durbin, T.J., Bateman, R.J., Benzinger, T.L.-S., Morris, J.C., Raichle, M.E., and Vlassenko, A.G. (2019). Persistent metabolic youth in the aging female brain. Proc. Natl. Acad. Sci. USA *116*, 3251–3255. https://doi.org/10.1073/pnas.1815917116.
8. O'Dwyer, L., Lamberton, F., Bokde, A.L.W., Ewers, M., Faluyi, Y.O., Tanner, C., Mazoyer, B., O'Neill, D., Bartley, M., Collins, R., et al. (2012). Sexual Dimorphism in Healthy Aging and Mild Cognitive Impairment: A DTI Study. PLoS One *7*, e37021. https://doi.org/10.1371/journal.pone.0037021.
9. Jack, C.R., Wiste, H.J., Weigand, S.D., Knopman, D.S., Vemuri, P., Mielke, M.M., Lowe, V., Senjem, M.L., Gunter, J.L., Machulda, M.M., et al. (2015). Age, sex and APOE ε4 effects on memory, brain structure and β-amyloid across the adult lifespan. JAMA Neurol. *72*, 511–519. https://doi.org/10.1001/jamaneurol.2014.4821.
10. Casaletto, K.B., Elahi, F.M., Staffaroni, A.M., Walters, S., Contreras, W.R., Wolf, A., Dubal, D., Miller, B., Yaffe, K., and Kramer, J.H. (2019). Cognitive Aging is Not Created Equally: Differentiating Unique Cognitive Phenotypes in "Normal" Adults. Neurobiol. Aging *77*, 13–19. https://doi.org/10.1016/j.neurobiolaging.2019.01.007.
11. Yang, J., Qu, J., and Ma, H. (2022). Recent developments in understanding brain aging: sex differences, mechanisms, and implications in diseases. Ageing Neur Dis *1*. https://doi.org/10.20517/and.2022.03.
12. Garigan, D., Hsu, A.L., Fraser, A.G., Kamath, R.S., Ahringer, J., and Kenyon, C. (2002). Genetic analysis of tissue aging in Caenorhabditis elegans: A role for heat-shock factor and bacterial proliferation. Genetics *161*, 1101–1112. https://doi.org/10.1093/genetics/161.3.1101.
13. Herndon, L.A., Schmeissner, P.J., Dudaronek, J.M., Brown, P.A., Listner, K.M., Sakano, Y., Paupard, M.C., Hall, D.H., and Driscoll, M. (2002). Stochastic and genetic factors influence tissue-specific decline in ageing C. elegans. Nature *419*, 808–814. https://doi.org/10.1038/nature01135.
14. Huang, C., Xiong, C., and Kornfeld, K. (2004). Measurements of age-related changes of physiological processes that predict lifespan of Caenorhabditis elegans. Proc. Natl. Acad. Sci. USA *101*, 8084–8089. https://doi.org/10.1073/pnas.0400848101.
15. Murakami, S., and Murakami, H. (2005). The effects of aging and oxidative stress on learning behavior in C. elegans. Neurobiol. Aging *26*, 899–905. https://doi.org/10.1016/j.neurobiolaging.2004.08.007.
16. Hughes, S.E., Evason, K., Xiong, C., and Kornfeld, K. (2007). Genetic and Pharmacological Factors That Influence Reproductive Aging in Nematodes. PLoS Genet. *3*, e25. https://doi.org/10.1371/journal.pgen.0030025.
17. Hodgkin, J., Horvitz, H.R., and Brenner, S. (1979). Nondisjunction Mutants of the Nematode CAENORHABDITIS ELEGANS. Genetics *91*, 67–94.
18. Cook, S.J., Jarrell, T.A., Brittin, C.A., Wang, Y., Bloniarz, A.E., Yakovlev, M.A., Nguyen, K.C.Q., Tang, L.T.-H., Bayer, E.A., Duerr, J.S., et al. (2019). Whole-animal connectomes of both Caenorhabditis elegans sexes. Nature *571*, 63–71. https://doi.org/10.1038/s41586-019-1352-7.
19. Portman, D.S. (2017). Sexual modulation of sex-shared neurons and circuits in C. elegans. J. Neurosci. Res. *95*, 527–538. https://doi.org/10.1002/JNR.23912.
20. White, J.Q., Nicholas, T.J., Gritton, J., Truong, L., Davidson, E.R., and Jorgensen, E.M. (2007). The Sensory Circuitry for Sexual Attraction in C. elegans Males. Curr. Biol. *17*, 1847–1857. https://doi.org/10.1016/j.cub.2007.09.011.
21. Fagan, K.A., Luo, J., Lagoy, R.C., Schroeder, F.C., Albrecht, D.R., and Portman, D.S. (2018). A Single-Neuron Chemosensory Switch Determines the Valence of a Sexually Dimorphic Sensory Behavior. Curr. Biol. *28*, 902–914.e5. https://doi.org/10.1016/j.cub.2018.02.029.
22. Lipton, J., Kleemann, G., Ghosh, R., Lints, R., and Emmons, S.W. (2004). Mate Searching in Caenorhabditis elegans: A Genetic Model for Sex Drive in a Simple Invertebrate. J. Neurosci. *24*, 7427–7434. https://doi.org/10.1523/JNEUROSCI.1746-04.2004.
23. Ryan, D.A., Miller, R.M., Lee, K., Neal, S.J., Fagan, K.A., Sengupta, P., and Portman, D.S. (2014). Sex, Age, and hunger regulate behavioral prioritization through dynamic modulation of chemoreceptor expression. Curr. Biol. *24*, 2509–2517. https://doi.org/10.1016/j.cub.2014.09.032.
24. Sammut, M., Cook, S.J., Nguyen, K.C.Q., Felton, T., Hall, D.H., Emmons, S.W., Poole, R.J., and Barrios, A. (2015). Glia-derived neurons are required for sex-specific learning in C. elegans. Nature *526*, 385–390. https://doi.org/10.1038/nature15700.
25. Tanner, D., Carigo, D., Sevilla, C., Lewis, M., and Harris, G. (2022). Sex differences in decision-making : Identifying multisensory behavioral differences in males and hermaphrodites. MicroPubl. Biol. *1*. https://doi.org/10.17912/2Fmicropub.biology.0005944–9.
26. Kauffman, A.L., Ashraf, J.M., Corces-Zimmerman, M.R., Landis, J.N., and Murphy, C.T. (2010). Insulin Signaling and Dietary Restriction Differentially Influence the Decline of Learning and Memory with Age. PLoS Biol.

8, e1000372. https://doi.org/10.1371/journal.pbio.1000372.
27. Arey, R.N., Stein, G.M., Kaletsky, R., Kauffman, A., and Murphy, C.T. (2018). Activation of G αq Signaling Enhances Memory Consolidation and Slows Cognitive Decline. Neuron *98*, 562–574.e5. https://doi.org/10.1016/j.neuron.2018.03.039.
28. Guo, X., Navetta, A., Gualberto, D.G., and García, L.R. (2012). Behavioral decay in aging male C. elegans correlates with increased cell excitability. Neurobiol. Aging *33*, 1483.e5. https://doi.org/10.1016/j.neurobiolaging.2011.12.016.
29. Kim, B., Suo, B., and Emmons, S.W. (2016). Gene Function Prediction Based on Developmental Transcriptomes of the Two Sexes in C. elegans. Cell Rep. *17*, 917–928. https://doi.org/10.1016/j.celrep.2016.09.051.
30. Ebbing, A., Vértesy, Á., Betist, M.C., Spanjaard, B., Junker, J.P., Berezikov, E., van Oudenaarden, A., and Korswagen, H.C. (2018). Spatial Transcriptomics of C. elegans Males and Hermaphrodites Identifies Sex-Specific Differences in Gene Expression Patterns. Dev. Cell *47*, 801–813.e6. https://doi.org/10.1016/j.devcel.2018.10.016.
31. Reilly, D.K., McGlame, E.J., Vandewyer, E., Robidoux, A.N., Muirhead, C.S., Northcott, H.T., Joyce, W., Alkema, M.J., Gegear, R.J., Beets, I., and Srinivasan, J. (2021). Distinct neuropeptide-receptor modules regulate a sex-specific behavioral response to a pheromone. Commun. Biol. *4*, 1018–1116. https://doi.org/10.1038/s42003-021-02547-7.
32. Shi, C., Runnels, A.M., and Murphy, C.T. (2017). Mating and male pheromone kill Caenorhabditis males through distinct mechanisms. Elife *6*, 234933–e23526. https://doi.org/10.7554/eLife.23493.
33. Torayama, I., Ishihara, T., and Katsura, I. (2007). Caenorhabditis elegans Integrates the Signals of Butanone and Food to Enhance Chemotaxis to Butanone. J. Neurosci. *27*, 741–750. https://doi.org/10.1523/JNEUROSCI.4312-06.2007.
34. Srinivasan, J., Kaplan, F., Ajredini, R., Zachariah, C., Alborn, H.T., Teal, P.E.A., Malik, R.U., Edison, A.S., Sternberg, P.W., and Schroeder, F.C. (2008). A blend of small molecules regulates both mating and development in Caenorhabditis elegans. Nature *454*, 1115–1118. https://doi.org/10.1038/nature07168.
35. Chatterjee, I., Ibanez-Ventoso, C., Vijay, P., Singaravelu, G., Baldi, C., Bair, J., Ng, S., Smolyanskaya, A., Driscoll, M., and Singson, A. (2013). Dramatic fertility decline in aging C. elegans males is associated with mating execution deficits rather than diminished sperm quality. Exp. Gerontol. *48*, 1156–1166. https://doi.org/10.1016/j.exger.2013.07.014.
36. Pan, C.L., Peng, C.Y., Chen, C.H., and McIntire, S. (2011). Genetic analysis of age-dependent defects of the Caenorhabditis elegans touch receptor neurons. Proc. Natl. Acad. Sci. USA *108*, 9274–9279. https://doi.org/10.1073/PNAS.1011711108.
37. Tank, E.M.H., Rodgers, K.E., and Kenyon, C. (2011). Spontaneous Age-Related Neurite Branching in Caenorhabditis elegans. J. Neurosci. *31*, 9279–9288. https://doi.org/10.1523/JNEUROSCI.6606-10.2011.
38. Toth, M.L., Melentijevic, I., Shah, L., Bhatia, A., Lu, K., Talwar, A., Naji, H., Ibanez-Ventoso, C., Ghose, P., Jevince, A., et al. (2012). Neurite Sprouting and Synapse Deterioration in the Aging Caenorhabditis elegans Nervous System. J. Neurosci. *32*, 8778–8790. https://doi.org/10.1523/JNEUROSCI.1494-11.2012.
39. Lakhina, V., Arey, R.N., Kaletsky, R., Kauffman, A., Stein, G., Keyes, W., Xu, D., and Murphy, C.T. (2015). Genome-wide functional analysis of CREB/long-term memory-dependent transcription reveals distinct basal and memory gene expression programs. Neuron *85*, 330–345. https://doi.org/10.1016/J.NEURON.2014.12.029.
40. Stein, G.M., and Murphy, C.T. (2014). C. elegans positive olfactory associative memory is a molecularly conserved behavioral paradigm. Neurobiol. Learn. Mem. *115*, 86–94. https://doi.org/10.1016/j.nlm.2014.07.011.
41. Wang, J., Kaletsky, R., Silva, M., Williams, A., Haas, L.A., Androwski, R.J., Landis, J.N., Patrick, C., Rashid, A., Santiago-Martinez, D., et al. (2015). Cell-Specific Transcriptional Profiling of Ciliated Sensory Neurons Reveals Regulators of Behavior and Extracellular Vesicle Biogenesis. Curr. Biol. *25*, 3232–3238. https://doi.org/10.1016/j.cub.2015.10.057.
42. Kaletsky, R., Lakhina, V., Arey, R., Williams, A., Landis, J., Ashraf, J., and Murphy, C.T. (2016). The C. elegans adult neuronal IIS/FOXO transcriptome reveals adult phenotype regulators. Nature *529*, 92–96. https://doi.org/10.1038/nature16483.
43. Kaletsky, R., Yao, V., Williams, A., Runnels, A.M., Tadych, A., Zhou, S., Troyanskaya, O.G., and Murphy, C.T. (2018). Transcriptome analysis of adult Caenorhabditis elegans cells reveals tissue-specific gene and isoform expression. PLoS Genet. *14*, e1007559. https://doi.org/10.1371/journal.pgen.1007559.
44. Weng, Y., Zhou, S., Morillo, K., Kaletsky, R., Lin, S., and Murphy, C.T. (2024). The Neuron-specific IIS/FOXO Transcriptome in Aged Animals Reveals Regulatory Mechanisms of Cognitive Aging. Elife *13*. https://doi.org/10.7554/eLife.95621.1.
45. Barr, M.M., and Sternberg, P.W. (1999). A polycystic kidney-disease gene homologue required for male mating behaviour in C. elegans. Nature *401*, 386–389. https://doi.org/10.1038/43913.
46. Ahn, S., Yang, H., Son, S., Lee, H.S., Park, D., Yim, H., Choi, H.-J., Swoboda, P., and Lee, J. (2022). The *C. elegans* regulatory factor X (RFX) DAF-19M module: A shift from general ciliogenesis to cell-specific ciliary and behavioral specialization. Cell Rep. *39*, 110661. https://doi.org/10.1016/j.celrep.2022.110661.
47. Kroetz, M.B., and Zarkower, D. (2015). Cell-Specific mRNA Profiling of the Caenorhabditis elegans Somatic Gonadal Precursor Cells Identifies Suites of Sex-Biased and Gonad-Enriched Transcripts. G3 (Bethesda). *5*, 2831–2841. https://doi.org/10.1534/g3.115.022517.
48. Miller, R.M., and Portman, D.S. (2010). A latent capacity of the C. elegans polycystins to disrupt sensory transduction is repressed by the single-pass ciliary membrane protein CWP-5. Dis. Model. Mech. *3*, 441–450. https://doi.org/10.1242/dmm.002816.
49. Sudmant, P.H., Lee, H., Dominguez, D., Heiman, M., and Burge, C.B. (2018). Widespread Accumulation of Ribosome-Associated Isolated 3′ UTRs in Neuronal Cell Populations of the Aging. Cell Rep. *25*, 2447–2456.e4. https://doi.org/10.1016/j.celrep.2018.10.094.
50. Chen, M., Lyu, G., Han, M., Nie, H., Shen, T., Chen, W., Niu, Y., Song, Y., Li, X., Li, H., et al. (2018). 3′ UTR lengthening as a novel mechanism in regulating cellular senescence. Genome Res. *28*, 285–294. https://doi.org/10.1101/gr.224451.117.
51. Portman, D.S. (2007). Genetic Control of Sex Differences in C. elegans Neurobiology and Behavior. Adv. Genet. *59*, 1–37. https://doi.org/10.1016/S0065-2660(07)59001-2.
52. Loxterkamp, E., Cha, J., Wu, K., Sullivan, J., Holbrook, O., Ghaith, H., Srun, L., and Bauer, D.E. (2021). Behavioral Differences between Male and Hermaphrodite C. elegans. MicroPubl. Biol. *2021*. https://doi.org/10.17912/micropub.biology.000431.
53. Madl, J.E., and Herman, R.K. (1979). Polyploids and sex determination in Caenorhabditis elegans. Genetics *93*, 393–402. https://doi.org/10.1093/genetics/93.2.393.
54. Meyer, B.J., and Casson, L.P. (1986). Caenorhabditis elegans compensates for the difference in X chromosome dosage between the sexes by regulating transcript levels. Cell *47*, 871–881. https://doi.org/10.1016/0092-8674(86)90802-0.
55. Albritton, S.E., Kranz, A.L., Rao, P., Kramer, M., Dieterich, C., and Ercan, S. (2014). Sex-biased gene expression and evolution of the X chromosome in nematodes. Genetics *197*, 865–883. https://doi.org/10.1534/GENETICS.114.163311/-/DC1/GENETICS.114.163311-13.XLS.
56. Esse, R., Gushchanskaia, E.S., Lord, A., and Grishok, A. (2019). DOT1L complex suppresses transcription from enhancer elements and ectopic RNAi in Caenorhabditis elegans. RNA *25*, 1259–1273. https://doi.org/10.1261/rna.070292.119.
57. Esse, R., and Grishok, A. (2020). Caenorhabditis elegans Deficient in DOT-1.1 Exhibit Increases in H3K9me2 at Enhancer and Certain RNAi-Regulated Regions. Cells *9*, 1846. https://doi.org/10.3390/cells9081846.
58. Sinclair, J., Pinter, K., Samuel, T., Beardsley, S., Yuan, X., Zhang, J., Meng, K., Yun, S., Krause, M., and Hamza, I. (2017). Inter-organ signaling by HRG-7 promotes systemic heme homeostasis. Nat. Cell Biol. *19*, 799–807. https://doi.org/10.1038/ncb3539.
59. Luo, S., Kleemann, G.A., Ashraf, J.M., Shaw, W.M., and Murphy, C.T. (2010). TGF-β and insulin signaling regulate reproductive aging via oocyte and germline quality maintenance. Cell *143*, 299–312. https://doi.org/10.1016/j.cell.2010.09.013.
60. Raichle, M.E., and Gusnard, D.A. (2002). Appraising the brain's energy budget. Proc. Natl. Acad. Sci. USA *99*, 10237–10239. https://doi.org/10.1073/pnas.172399499.
61. Demarest, T.G., and McCarthy, M.M. (2015). Sex differences in mitochondrial (dys) function: Implications for neuroprotection. J. Bioenerg. Biomembr. *47*, 173–188. https://doi.org/10.1007/s10863-014-9583-7.
62. Johri, A., and Beal, M.F. (2012). Mitochondrial Dysfunction in Neurodegenerative Diseases. J. Pharmacol. Exp. Ther. *342*, 619–630. https://doi.org/10.1124/jpet.112.192138.
63. Mor, D.E., Sohrabi, S., Kaletsky, R., Keyes, W., Tartici, A., Kalia, V., Miller, G.W., and Murphy, C.T. (2020). Metformin rescues Parkinson's disease phenotypes caused by hyperactive mitochondria. Proc. Natl. Acad. Sci. USA *117*, 26438–26447. https://doi.org/10.1073/pnas.2009838117.
64. Taylor, S.R., Santpere, G., Weinreb, A., Barrett, A., Reilly, M.B., Xu, C., Varol, E., Oikonomou, P., Glenwinkel, L., McWhirter, R.,

et al. (2021). Molecular topography of an entire nervous system. Cell *184*, 4329–4347.e23. https://doi.org/10.1016/j.cell.2021.06.023.

65. Bakker, A., Krauss, G.L., Albert, M.S., Speck, C.L., Jones, L.R., Stark, C.E., Yassa, M.A., Bassett, S.S., Shelton, A.L., and Gallagher, M. (2012). Reduction of Hippocampal Hyperactivity Improves Cognition in Amnestic Mild Cognitive Impairment. Neuron *74*, 467–474. https://doi.org/10.1016/j.neuron.2012.03.023.
66. Appiah, B., Fullio, C.L., Ossola, C., Bertani, I., Restelli, E., Cheffer, A., Polenghi, M., Haffner, C., Garcia-Miralles, M., Zeis, P., et al. (2023). DOT1L activity affects neural stem cell division mode and reduces differentiation and ASNS expression. EMBO Rep. *24*, e56233. https://doi.org/10.15252/embr.202256233.
67. Van Heesbeen, H.J., Von Oerthel, L., De Vries, P.M., Wagemans, C.M.R.J., and Smidt, M.P. (2023). Neuronal Dot1l Activity Acts as a Mitochondrial Gene-Repressor Associated with Human Brain Aging via H3K79 Hypermethylation. Int. J. Mol. Sci. *24*, 1387. https://doi.org/10.3390/ijms24021387.
68. Berletch, J.B., Yang, F., and Disteche, C.M. (2010). Escape from X inactivation in mice and humans. Genome Biol. *11*, 213. https://doi.org/10.1186/gb-2010-11-6-213.
69. Shaw, C.K., Abdulai-Saiku, S., Marino, F., Wang, D., Davis, E.J., Panning, B., and Dubal, D.B. (2023). X Chromosome Factor Kdm6a Enhances Cognition Independent of Its Demethylase Function in the Aging XY Male Brain. J. Gerontol. A Biol. Sci. Med. Sci. *78*, 938–943. https://doi.org/10.1093/gerona/glad007.
70. Galaxy Community (2022). The Galaxy platform for accessible, reproducible and collaborative biomedical analyses: 2022 update. Nucleic Acids Res. *50*, W345–W351. https://doi.org/10.1093/nar/gkac247.
71. Andrews, S. (2010). FastQC: A Quality Control Tool for High Throughput Sequence Data. http://www.bioinformatics.babraham.ac.uk/projects/fastqc/.
72. Dobin, A., Davis, C.A., Schlesinger, F., Drenkow, J., Zaleski, C., Jha, S., Batut, P., Chaisson, M., and Gingeras, T.R. (2013). STAR: ultrafast universal RNA-seq aligner. Bioinformatics *29*, 15–21. https://doi.org/10.1093/bioinformatics/bts635.
73. Anders, S., Pyl, P.T., and Huber, W. (2015). HTSeq—a Python framework to work with high-throughput sequencing data. Bioinformatics *31*, 166–169. https://doi.org/10.1093/bioinformatics/btu638.
74. Love, M.I., Huber, W., and Anders, S. (2014). Moderated estimation of fold change and dispersion for RNA-seq data with DESeq2. Genome Biol. *15*, 550. https://doi.org/10.1186/s13059-014-0550-8.
75. Anders, S., Reyes, A., and Huber, W. (2012). Detecting differential usage of exons from RNA-seq data. Genome Res. *22*, 2008–2017. https://doi.org/10.1101/GR.133744.111.
76. Holdorf, A.D., Higgins, D.P., Hart, A.C., Boag, P.R., Pazour, G.J., Walhout, A.J.M., and Walker, A.K. (2020). WormCat: An online tool for annotation and visualization of caenorhabditis elegans genome-scale data. Genetics *214*, 279–294. https://doi.org/10.1534/genetics.119.302919.
77. Raudvere, U., Kolberg, L., Kuzmin, I., Arak, T., Adler, P., Peterson, H., and Vilo, J. (2019). g:Profiler: a web server for functional enrichment analysis and conversions of gene lists (2019 update). Nucleic Acids Res. *47*, W191–W198. https://doi.org/10.1093/nar/gkz369.
78. Schindelin, J., Arganda-Carreras, I., Frise, E., Kaynig, V., Longair, M., Pietzsch, T., Preibisch, S., Rueden, C., Saalfeld, S., Schmid, B., et al. (2012). Fiji: an open-source platform for biological-image analysis. Nat. Methods *9*, 676–682. https://doi.org/10.1038/nmeth.2019.
79. Kauffman, A., Parsons, L., Stein, G., Wills, A., Kaletsky, R., and Murphy, C. (2011). C. elegans positive butanone learning, short-term, and long-term associative memory assays. J. Vis. Exp. 2490–2499. https://doi.org/10.3791/2490.
80. Zhou, S., Zhang, Y., Kaletsky, R., Toraason, E., Zhang, W., Dong, M.-Q., and Murphy, C.T. (2023). Signaling from the C. elegans Hypodermis Non-autonomously Facilitates Short-term Associative Memory. Preprint at bioRxiv *1*. https://doi.org/10.1101/2023.02.16.528821.
81. Wan, X., Zhou, Y., Chan, C.M., Yang, H., Yeung, C., and Chow, K.L. (2019). SRD-1 in AWA neurons is the receptor for female volatile sex pheromones in C. elegans males. EMBO Rep. *20*, e46288. https://doi.org/10.15252/embr.201846288.

STAR★METHODS

KEY RESOURCES TABLE

REAGENT or RESOURCE	SOURCE	IDENTIFIER
Bacterial and virus strains		
OP50 *E. Coli* (BactoBeads)	Sigma-Aldrich	Cat. #S29021
HT115 E coli	Caenorhabditis Genetics Center	RRID:WB-STRAIN:WBStrain00041079
Chemicals, peptides, and recombinant proteins		
2-Butanone, 99+%, extra pure	Acros Organics	Cat. #149670250
Benzaldehyde	Millipore Sigma	Cat. #B1334-100G
Pyrazine	Sigma-Aldrich	Cat. #P56003-5G
Leibovitz's L-15 Medium, no phenol red	Gibco	Cat. #21083027
Protease from Streptomyces griseus	Sigma-Aldrich	Cat. #P8811-1G
Fetal Bovine Serum	Gibco	Cat. #16140089
Sodium dodecyl sulfate	Millipore Sigma	Cat. #C988X47
DTT	Millipore Sigma	Cat. # 3483-12-3
HEPES 1M Buffer, pH 8.0	Thermo Fisher Scientific	Cat. #AAJ63578AK
TRIzol Reagent	Thermo Fisher Scientific	Cat. #15596026
Chloroform	Sigma-Aldrich	Cat. #288306-100mL
2-propanol	Sigma-Aldrich	Cat. #I9516-25mL
Sigma Protector RNase inhibitor	Sigma-Aldrich	Cat. #3335402001
Critical commercial assays		
Ovation SoLo RNA-Seq library preparation kit	Tecan Genomics	REF # 0407-32
SOLO Anydeplete Custome Probe Mix for C. elegans, IC0149S	Tecan Genomics	REF# S02253
RNeasy MinElute Cleanup Kit	Qiagen	Cat. # 74204
RNase-free DNase set	Qiagen	Cat. # 79254
Deposited data		
RNA-seq data	This Paper	NCBI BioProject: PRJNA1054152
Experimental models: Organisms/strains		
C. elegans strain N2 var. Bristol: wild type	Caenorhabditis Genetics Center	RRID:WB-STRAIN:WBStrain00000003
C. elegans strain CB1489: *him-8(e1489) IV*	*C. elegans* Genome Center	RRID:WB-STRAIN:WBStrain00004346
C. elegans strain CQ675: *daf-22(m130) II; him-8(e1489) IV*	This Paper	CQ675
C. elegans strain CQ676: *daf-22(m130) II; him-8(e1489) IV; otIs45 [Punc-119::GFP] V*	This Paper	CQ676
C. elegans strain PB4641: *C. remanei*	*C. elegans* Genome Center	RRID:WB-STRAIN:WBStrain00041998
C. elegans strain TU3595: *sid-1(pk3321) him-5(e1490) V; lin-15B(n744) X; uIs72 [pCFJ90(Pmyo-2::mCherry) + Punc-119::sid-1 + Pmec-18::mec-18::GFP]*	*C. elegans* Genome Center	RRID:WB-STRAIN:WBStrain00035060
C. elegans strain CQ743: *kyIs140 [str-2::GFP + lin-15(+)] I; daf-22(m130) II; him-8(e1489) IV*	This Paper	CQ743
C. elegans strain CZ10175: *zdIs5 [mec-4p::GFP + lin-15(+)] I*	*C. elegans* Genome Center	RRID:WB-STRAIN:WBStrain00005421

(*Continued on next page*)

Continued

REAGENT or RESOURCE	SOURCE	IDENTIFIER
Oligonucleotides		
daf-22(m130) wild-type super selective forward primer 5′- GGGTGATCAATCCATCCGGA GGGAACTACTCGAAGG -3′	This Paper	N/A
daf-22(m130) mutant super selective forward primer 5′- GGGTGATCAATCCATCCGCA CGGAACTACTCGAAGA -3′	This Paper	N/A
daf-22(m130) genotyping reverse primer 5′- GCCAGTAGAAGTCTGGAGGCG -3′	This Paper	N/A
daf-22 sequence forward primer 5′- TCTACGACTTTATGGGTCTCCTCG -3′	This Paper	N/A
daf-22 sequence reverse primer 5′- CACTTGTCTCTTTCCACATTTGCC -3′	This Paper	N/A
Recombinant DNA		
Plasmid pL4440 RNAi	Addgene	RRID:Addgene_1654
Plasmid: pL4440-*acdh-1* RNAi	Ahringer	*acdh-1*
Plasmid: pL4440-*nlp-20* RNAi	Ahringer	*nlp-20*
Plasmid: pL4440-*hrg-7* RNAi	Ahringer	*hrg-7*
Plasmid: pL4440-*lin-42* RNAi	Ahringer	*lin-42*
Software and algorithms		
GraphPad Prism version 8.0 or 9.0	GraphPad Software	https://www.graphpad.com
Galaxy version 21.05	The Galaxy Community, 2022[70]	https://galaxy.princeton.edu/
FastQC	Andrews, 2010[71]	https://www.bioinformatics.babraham.ac.uk/projects/fastqc/
RNA-STAR	Dobin et al., 2013[72]	https://code.google.com/archive/p/rna-star/
htseq-count	Anders et al., 2015[73]	https://htseq.readthedocs.io/en/release_0.11.1/count.html
DESeq2 v1.28	Love et al., 2014[74]	https://github.com/emc2cube/Bioinformatics/
DEXSeq	Anders et al., 2012[75]	https://bioconductor.org/packages/release/bioc/html/DEXSeq.html
Tissue query	Kaletsky et al., 2018[43]	https://worm.princeton.edu/
Wormcat 2.0	Holdorf et al., 2020[76]	http://www.wormcat.com/
g:Profiler	Raudvere et al., 2019[77]	https://biit.cs.ut.ee/gprofiler/gost
FIJI ImageJ	Schindelin et al., 2012[78]	https://imagej.net/software/fiji/

RESOURCE AVAILABILITY

Lead contact

Further information and requests for resources and reagents should be directed to and will be fulfilled by the lead contact, Coleen T. Murphy (ctmurphy@princeton.edu).

Materials availability

Worm strains generated in this study are available upon request. This study did not generate new unique reagents.

Data and code availability

- The raw sequence data are available in the public database (https://www.ncbi.nlm.nih.gov/bioproject/) under the BioProject, PRJNA1054152. The accession number for the dataset is listed in the key resources table. Microscopy data reported in this paper will be shared by the lead contact upon request.

- This paper does not report original code.
- Any additional information required to reanalyze the data reported in this paper is available from the lead contact upon request.

EXPERIMENTAL MODEL AND STUDY PARTICIPANT DETAILS

General worm maintenance

All strains are maintained using standard methods. *C. elegans* are maintained at 20°C on high growth media (HGM, 3 g/L NaCl, 20 g/L Bacto-peptone, 30 g/L Bacto-agar in distilled water, with 4 mL/L cholesterol (5 mg/mL in ethanol), 1 mL/L 1M CaCl2, 1 mL/L 1M MgSO4, and 25 mL/L 1M potassium phosphate buffer (pH 6.0) added to molten agar after autoclaving) or normal growth media (NGM, HGM recipe modified as follows: 2.5 g/L Bacto-peptone, 17 g/L Bacto-agar, and 1 mL/L cholesterol (5 mg/mL in ethanol); all other components same as HGM) seeded with OP50 bacteria (CGC). To synchronize worms, gravid adult Day 2 worms are treated with 15% sodium hypochlorite solution (80 mL ddH2O, 15 mL NaOCl, 5 mL KOH) for 8 min, or until 80% of worm body are invisible, to obtain synchronized eggs and avoid overbleaching. Synchronized eggs are directly put on seeded HGM or NGM plates and allowed to grow. For RNA interference assays, worms are grown on HGM plates until L4, and then transferred onto HGM with 1 mM IPTG and 100 mg/L Carbenicilin plates seeded with respective HT115 RNAi bacteria from the Ahringer Library. For experiments with aged worms, worms are transferred onto plates supplemented with 50 μM Floxuridine (FUDR) starting from L4. Worms are transferred to plates without FUDR at least 1 day before behavioral experiments. For experiments where a pure male population is needed, mixed Day 1 adult male and hermaphrodites are washed off plates with M9 and additionally washed 2 times before freely passing through a 35 mm nylon mesh filter for 10 min to separate males from hermaphrodites, and are rested for 1 day before performing experiments. Males and hermaphrodites are then examined under a microscope for filtration success. A 95% male purity is needed for further experiments.

C. elegans strains

CB1489: *him-8(e1489) IV*,
CQ675: *daf-22(m130) II; him-8(e1489) IV*,
CQ676: *daf-22(m130) II; him-8(e1489) IV; otIs45 [Punc-119::GFP] V*,
PB4641: *C. remanei*,
TU3595: *sid-1(pk3321) him-5(e1490) V; lin-15B(n744) X; uIs72 [pCFJ90(Pmyo-2::mCherry) + Punc-119::sid-1 + Pmec-18::mec-18::GFP]*,
CQ743: *kyIs140 [str-2::GFP + lin-15(+)] I; daf-22(m130) II; him-8(e1489) IV*.
CZ10175: *zdIs5 [mec-4p::GFP + lin-15(+)] I*.

METHOD DETAILS

Chemotaxis and learning and memory assays

The learning and memory assays were performed as previously described.[26,40,42,44,79,80] Briefly, chemotaxis assays toward 10% butanone were performed for both naive untrained worms and trained worms left on holding plates for various amounts of time to identify naive chemotaxis, learning, and memory, respectively. Chemotaxis plates were prepared by placing 1 μL of 10% butanone diluted in ethanol and 1 μL of 100% ethanol on two spots 80 mm apart on unseeded 100 mm NGM plates. Each spot also had 1 μL of 7.5% NaN3 to immobilize the worms. Worms were washed off plates with M9 and washed 2 additional times to remove residual bacteria before being put on chemotaxis plates on a spot 5.5 cm away from either the butanone or ethanol spots and given 1 h to chemotaxis to butanone or ethanol spots. Chemotaxis was measured as below

$$Chemotaxis\ Index\ (CI) = \frac{\#\ of\ worms\ at\ butanone - \#\ of\ worms\ at\ ethanol}{total\ \#\ of\ worms - \#\ of\ worms\ at\ origin}$$

The learning index was calculated as below

$$Learning\ Index\ (LI) = CI_{trained} - CI_{naive}$$

Naive worms were tested for chemotaxis toward butanone without training. Learning and memory were measured using worms trained on seeded NGM plates with 18 μL butanone separated into 4 streaks on the lid for an hour. Learning was assessed immediately after training, while 1-h and 2-h memory were evaluated by placing worms on seeded holding plates without butanone streaks for 1 h or 2 h before measuring chemotaxis, respectively.

For learning and memory assays involving male worms, male specimens were filtered a day before the experiment to ensure recovery from filtration.

For pyrazine and benzaldehyde chemotaxis assays, the procedure was similar to the naive chemotaxis assay, except 1 μL of 10% pyrazine diluted in ethanol or 1uL of 1% benzaldehyde diluted in ethanol was used instead of 10% butanone.

Pheromone preference assay

Pheromone preference assays were performed similar to previously described.[20,32,81] For the pheromone preference assay, we used *C. remanei* true female pheromone because it had been shown to be more attractive than hermaphrodite pheromone.[81] *C. remanei*

pheromone was collected by separating L4 males or females onto seeded plates without the opposing sex until Day 4. Then Day 4 worms were picked into M9 with a concentration of 10 worms/100μL M9. Worms were kept in M9 overnight to collect pheromone. For pheromone chemotaxis plates, 2uL of pheromone solution and M9 solution were dotted on 2 different spots separated 5 cm apart on a 60 mm unseeded NGM plate. Each spot also had 1 uL of 7.5% NaN_3 solution to immobilize worms once they reached the spot. Chemotaxis assays to pheromone were performed similarly to chemical chemotaxis assays. Males are washed onto chemotaxis plates and given 1 h to chemotaxis to either spot. The Chemotaxis Index was measured as chemical chemotaxis assays.

Neuron morphology imaging

We transferred synchronized worms to FUDR at L4 and maintained them by transferring them to fresh plates every 2 days. We imaged worms on adult Day 2, Day 8 and Day 12, using Nikon AXR confocal microscope's GFP channel at 60× magnification and 0.5 μm z stack. Images were processed using NIS-Elements and FIJI software and blindly quantified. For AWC neuron imaging, beading was measured as bead-like varicosities in the neurite, and wavy neurites were measured as significant path changes from normal neurite processes. For touch receptor neuron imaging, morphology blebbing was measured as intrusions from the neurites; branching was measured as the formation of clear neurite branches from the normal neurite; and wavy neurites are counted as significant path deviation from normal neurite processes. Imaging was performed in 3 biological replicates. Data analysis was performed using Prism software, and Chi-square statistical measurements were used.

Neuron sorting and RNA extraction

Neuron sorting and RNA extraction were performed as previously described.[42,43] For each biological replicate, 8 synchronized HGM plates of male worms were filtered to obtain a >95% pure male population on Day 1, and neuron sorting was performed on Day 2 and Day 8. Briefly, lysis buffer (200 mM DTT, 0.25% SDS, 20 mM HEPES pH 8.0, 3% sucrose dissolved in water) was used to break the cuticle, and then 20 mg/mL pronase solution from Streptomyces griseus accompanied by mechanical disruption was used to isolate single cells from the tissue. Cells are suspended in L-15 butter with 2% Fetal Bovine Serum (FBS) and kept at 4C throughout the sorting procedure. Cells are sorted using a FACSVantage SE w/DiVa (BD Biosciences; 488 nm excitation, 530/30 nm bandpass filter for GFP detection). We determined sorting gates by comparing with age-matched, genotype-matched non-fluorescent samples. The sorting process lasts about 40 min. Fluorescent neuron cells were directly sorted into Trizol. 100,000 GFP+ cells were collected for each sample. We collected six biological replicates for each age and sex. We used standard trizol-chloroform-isopropanol procedure for RNA extraction, and RNeasy MinElute Cleanup Kit (Qiagen) for RNA cleanup. RNA quality and concentration were then measured by Qubit and Agilent Bioanalyzer RNA Pico chip.

RNA sequencing and data analysis

Library preparation was performed using Ovation SoLo RNA-Seq library preparation kit with AnyDeplete Probe Mix- *C. elegans* (Tecan Genomics) with manufacturer's instructions and 2 ng of RNA input was used. Library quality and concentration were assessed using an Agilent Bioanalyzer DNA 12000 chip. Then we multiplexed the samples and performed sequencing using the NovaSeq S1 100 nt Flowcell v1.5 (Illumina).

Sequencing data analysis was conducted using the Galaxy website. FastQC was applied to each sample for quality control analysis. The RNA STAR package mapped reads to the *C. elegans* genome (ce11, UCSC Feb 2013) using the gene model ws245genes.gtf, resulting in 50–70% of reads being uniquely mapped. Reads that uniquely mapped to the genome were counted using the htseq-count algorithm in union mode. DESeq2 analysis was then employed for read normalization and differential expression analysis of the counted reads.[74] PCA analysis was performed along with the DESeq2 package. Genes with a $\log_2$(fold-change) > 1 and p-adjusted <0.05 were considered differentially expressed in subsequent analysis.

Gene ontology analysis was performed using either gprofiler[77] or WormCat 2.0[76] category 2. Tissue queries were performed on the top 500 highest fold-change genes, using the worm tissue query website (www.worm.princeton.edu),[43] and only major systems were selected in the analysis. The location, transcript and gene length of each gene is obtained from the Wormbase using the Wormmine. Transcript per million is calculated as below

$$TPMi = \frac{10^6 \times \left(\frac{c_i}{L_i/1000}\right)}{\sum_j \left(\frac{c_j}{L_j/1000}\right)}$$

Where TPMi is the Transcripts Per Million for the i-th gene, Ci is the read count for the i-th gene, and Li is the length of the i-th gene in base pairs.

Differential exon usage results were performed using the DEXSeq package version 1.28.1.0 on Galaxy. The Gene model of exons is flattened from the gene model ws245genes.gtf. We then ran DEXSeq count algorithms on the RNA-STAR bam count file on each sample, and used DEXSeq algorithm to analyze exon usage. Exons with a $\log_2$(fold-change) > 1 and p-adjusted <0.05 were considered differentially expressed in subsequent analyses. Representative gene exon usage graphs are generated using the plotdexseq function to plot exons and their normalized counts, and transcripts are shown below the graph. For analyzing differentially expressed CDS and UTRs, positions of CDS were

provided in the gene model ws245genes, and UTRs were calculated as all parts of the exon before the start codon (not including the start codon) or after the stop codon (including the stop codon).

QUANTIFICATION AND STATISTICAL ANALYSIS

Experimental analyses were analyzed using the Prism 10 software. two-way ANOVA with Tukey post-hoc tests were used to compare the learning curve or pheromone preference curve between multiple conditions. One-way ANOVA followed by Dunnet post-hoc tests for multiple comparisons was performed to compare chemotaxis index between control and experimental conditions. Chi-square test was performed to compare the neuron morphology change between young and aged AWC neurons. All GO term analysis were perform using gprofiler with adjusted *p*-values or Wormcat 2.0 software with Bonferroni corrected adjusted *p*-values as noted in the Fig. legend. Venn diagram overlaps were compared using the hypergeometric test. Differential expression analysis of RNA-seq and PCA were performed using the DESeq2 algorithm and adjusted *p*-values were generated with the Wald test using the Benjamini and Hochberg method (BH-adjusted *p*-values). Additional statistical details of experiments, including sample size (with n representing the number of chemotaxis assays performed for behavior, sample collections for RNA-seq, and the number of worms for microscopy), can be found in the methods and figure legends. Linear regression, Pearson's sorrelations and skewness were calculated using the python sklearn and SciPy packages. Skewness is calculated from the distribution histogram of hermaphrodite log(TPM+1) – male log(TPM+1) values.